Journal of Geosciences, Osaka City University
Vol. 41, Art. 6, p.85-107, March, 1998

Exsolution features in pyroxene phenocrysts from an anorthosite massif in northern Kerala, South India

H.M. RAJESH[1)*], M. SANTOSH[2)] AND M. YOSHIDA[1)]

1) Department of Geosciences, Faculty of Science, Osaka City University, Sugimoto 3-3-138, Sumiyoshi-ku, Osaka 558-8585, Japan
2) Centre for Earth Science Studies, PB 7250, Thuruvikkal Post, Trivandrum 695 031, India

Abstract

Peculiar exsolution features occur in pyroxene phenocrysts from the Perinthatta anorthosite massif in northern Kerala, South India. Optical microscopy, combined with color imaging methods using energy dispersive X-ray studies of both clinopyroxene and orthopyroxene phenocrysts, indicate that they show exsolution intergrowth of plagioclase together with Fe-Ti oxides. Substantial amounts of exsolved orthopyroxene in clinopyroxene and clinopyroxene in orthopyroxene were also observed. The occurrence of exsolution (rather inversion) features like inverted pigeonite, herring-bone type of exsolution, and diallage were noticed in these pyroxene phenocrysts. Oxide inclusions, usually found as separate grains scattered through the host pyroxene, show prominent occurrence as small arrays of particles exsolved in orientations that are semi-coherent with the pyroxene. Biotite occurs with pyroxene phenocrysts, locally as an integral portion of exsolution lamellae, as a probable exsolution phase (?). The widths of exsolution lamellae vary from micrometer to nanometer scale, with the lamellae of the same generation having nearly the same width. All phases in lamellae are crystallographically oriented in the pyroxene hosts and are essentially those of the planes of best fit at nucleation. The various silicate exsolution features are consistent with slow cooling of the pyroxene, resulting in coherent exsolution by heterogeneous nucleation and growth of the precipitate, with the oxide particles interpreted as the homogeneously nucleated analogue of the first. The association of oxide inclusions suggests that oxidizing conditions played an important role in controlling the properties and compositions of these phenocrysts. The various exsolution features documented here are indicative of a high initial crystallization temperature and also a high degree of cooling history for the anorthosite mass.

*corresponding author's e-mail address: rajesh@sci.osaka-cu.ac.jp

Key words: Anorthosite massif, pyroxene phenocrysts, exsolution lamellae, inverted pigeonite, nucleation and growth.

Introduction

Pyroxene phenocrysts containing exsolution features represented by intergrowths of composite lamellae of plagioclase and iron-titanium oxides, with additional lamellae of orthopyroxene or clinopyroxene, have been reported from a number of massif-type anorthosite complexes. Considering their crystallographically controlled orientation and difficulty in visualizing their precipitation from a melt following the kinetics of oxide nucleation and growth, these lamellae are generally agreed to be of exsolution origin. Exsolution lamellae are a direct fossil record of the conditions where the lamellae nucleated from the host, and can help in tracing the crystallization histories of the host rocks in which they are now found. Large single crystals of pyroxene (pyroxene phenocrysts) containing different types of exsolution lamellae, occurring commonly in anorthosite massifs and insignificant volumetrically, figure prominently in recent models for the origin and crystallization history of anorthositic rocks (Emslie, 1975; Morse, 1975; Bohlen and Essene, 1978; Dymek and Gromet, 1984; Owens and Dymek, 1995). As a further contribution towards unravelling the peterogenetic significance of pyroxene phenocrysts in massif-type anorthosites, the pres-

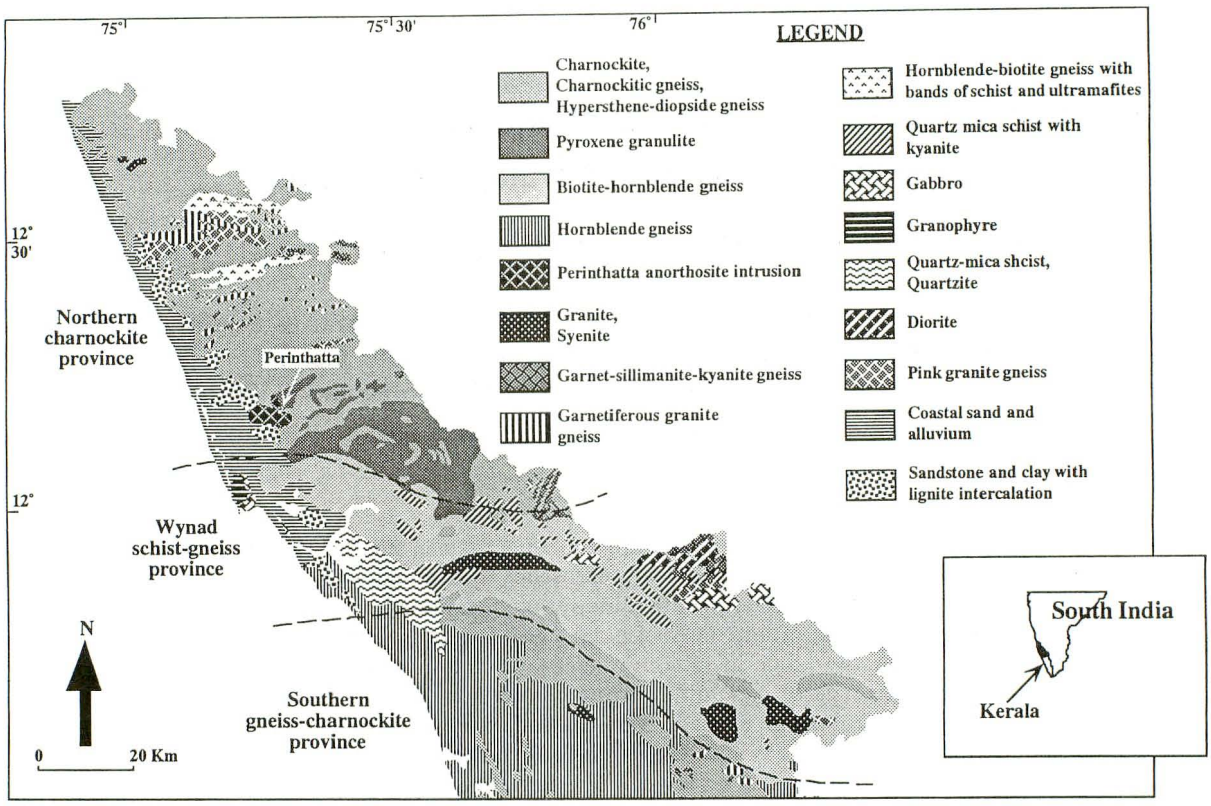

Fig. 1. Generalized geologic map of northern Kerala, South India, showing the distribution of various lithologies and the Perinthatta anorthosite intrusion (modified from GSI, 1995). The broad division of northern Kerala into three petrologic provinces is also shown. Inset shows the general outline of South India showing the location of northern Kerala.

ent paper gives a comprehensive account of the various exsolution features observed in pyroxene phenocrysts from an anorthosite massif in South India. Considering the complexity of exsolution features preserved, we also try to evaluate the possible general mechanism of exsolution. The documentation of such critical features have a wider implication in evaluating the thermal history of the host rock.

Geologic setting and field relations

Southern Peninsular India, characterized by the South Indian high-grade metamorphic terrain and the Eastern Ghats granulite belt, have many prominent occurrences of massif-type anorthosite. The granulite terrain of northern Kerala belong to the South Indian high-grade metamorphic terrain. It can be broadly divided into three major geologic regions, viz., northern charnockite province, Wynad schist-gneiss province, and gneiss/charnockite province south of Wynad schist-gneiss province (Fig. 1). Orthopyroxene-hornblende-biotite bearing intermediate to acid charnockites, basic granulites, hornblende/biotite-bearing gneisses, metasedimentary schists, igneous plutons of granite, syenite, anorthosite and gabbro, and minor tertiary sedimentary deposits constitute the dominant lithologies encountered in northern Kerala (Fig. 1). The samples for the present study were collected from an anorthosite mass confined to Perinthatta and its adjoining areas which occur within Kannur district, northern Kerala (Fig. 1). It is located between longitudes 75° 12′ and 75° 20′ E and latitudes 12° 7′ and 12° 14′ N and is represented in the Survey of India topo sheets 48P/4 and 48P/8 (Fig. 2). The Perinthatta anorthosite intrusion (having a roughly oval shape in map view), first reported by Vidyadharan et al. (1976), is emplaced within the northern charnockite province and is spatially associated with the Wynad schist-gneiss province (Fig. 1) and the Bavali lineament. The anorthosite occupy the core of the intrusion and extend towards the eastern margin, with more mafic variants encountered toward the margin. The anorthosite grades from anorthositic to gabbroic (noritic) anorthosite to anorthositic gabbro (norite) from core toward margin, and is

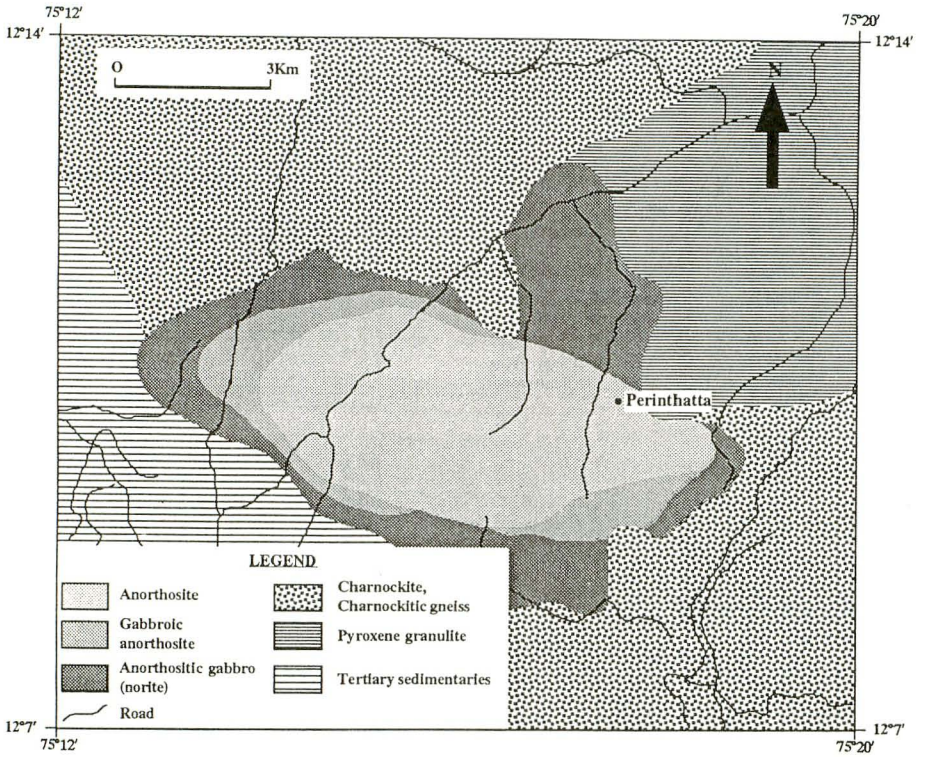

Fig. 2. Geological map of Perinthatta and its adjoining areas showing the distribution of the anorthosite mass. The anorthosite body grades from anorthositic core to gabbroic (noritic) anorthosite to anorthositic gabbro (norite) towards the margin. This classification is based on modal analysis and thin section studies. There is uncertainity regarding the exact contact between different geologic units due to extensive laterization and poor exposures and hence most of the contacts have been inferred.

massive in appearance. This gradation of anorthositic rocks was not possible to separate as mappable units on the geologic map of Perinthatta due to the comparable dark color of these rocks. But an attempt is made to delineate the possible relation between these rocks based on their modal analysis and thin section studies (Fig. 2). There is uncertainty regarding the exact extent of the pluton as the rock mass is extensively mantled by laterites and Tertiary rocks. The anorthosite is dark greenish to dark gray, with a greasy look on fresh surfaces, and coarse to medium grained, having ophitic to subophitic textures. A crude alignment of plagioclase megacrysts (trending E-W) was observed in most of the exposures. Macroscopically gabbroic anorthosite and norite resembles the anorthosite. They are similar in color and are generally coarse grained.

Petrography

The anorthosite is composed dominantly of plagioclase (mostly unzoned) cumulus crystals of labradorite-andesine composition and intercumulus minerals. The latter are mainly pyroxenes with high-Ca pyroxene constituting the most frequent, followed by low-Ca pyroxene, and Fe-Ti oxides, apatite, olivine, biotite, hornblende, K-feldspar and zircon completing the suite of accessory minerals. Rarely the two pyroxenes occur in equal proportions. Rare quartz was present in some of the samples. The mineral assemblage and modal proportions of the phases (Figs. 3a & b) distinguish the anorthosite body as anorthositic to gabbroic (noritic) anorthosite to anorthositic gabbro (norite), from core towards the margin (Fig. 2).

Plagioclase, which is usually the first mineral to crystallize, rarely exhibits polysynthetic twinning. The occurrence of antiperthitic lamellae is a common feature in all the samples studied. Based on the grain size and the complexity of exsolution features preserved, pyroxenes were distinguished as pyroxene phenocrysts (Figs. 4a, b, 5a & b) and matrix pyroxene. Both clinopyroxene (4-10 per cent) and orthopyroxene (2-6 per cent) occur in various forms: as relatively large (mostly $>$ 0.02 cm, rarely upto 1.5 cm) subhedral crystals (described here as pyroxene phenocrysts), in intergrowths with oxide minerals, as orthopyroxene

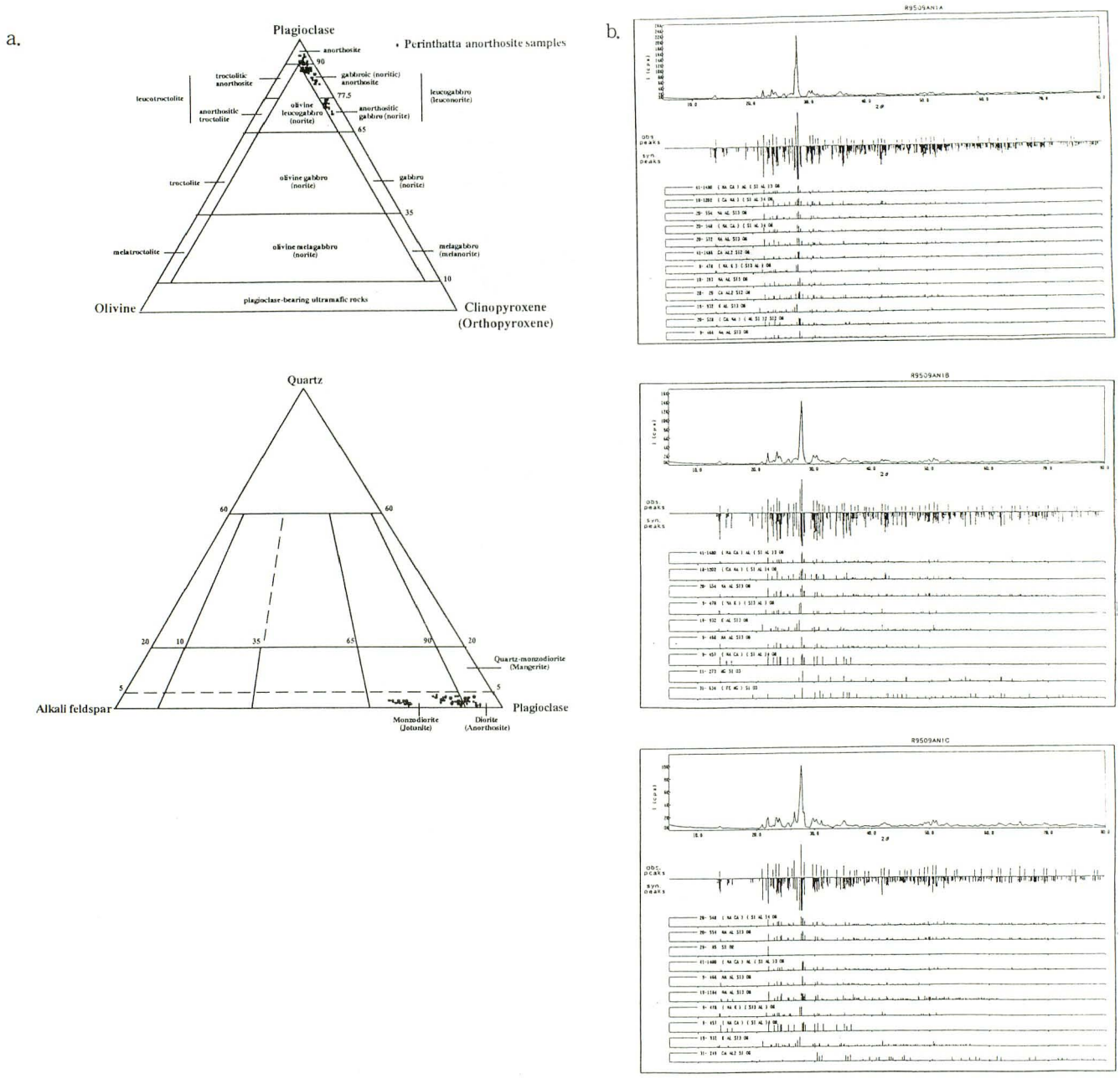

Fig. 3. a. Modal composition of anorthosite samples by point counting and whole-XRD analysis. Perinthatta anorthosite samples range from anorthosite to gabbroic (noritic) anorthosite to anorthositic gabbro (norite) in composition in the Streckeisen (1976) classification diagram of anorthositic rocks, while they have dioritic (anorthositic) to monzodioritic (jotunitic) composition in the Quartz-Alkali feldspar-Plagioclase diagram.
b. Representative whole-rock XRD analyses of Perinthatta anorthosite samples.

rims around clinopyroxene crystals and vice-versa, as rare orthopyroxene rims around olivine, and as small, granular crystals (described here as matrix pyroxene), usually associated with non-exsolved, equigranular grains of plagioclase. These pyroxenes are typically intergrown with plagioclase in ophitic or subophitic textures. The low-Ca pyroxenes have been identified as mostly ferrosilite to pigeonite while the high-Ca pyroxenes are mostly augite to ferroaugite (Rajesh, submitted). All the samples investigated contain 2-4 per cent oxides as discrete grains, situated together in the interstices of the silicates tightly fitting their contours (Figs. 4a, b, 5a & b); they have been identified as either magnetite, ilmenite, haematite or rutile (Rajesh, submitted). Euhedral to subhedral crystals of apatite usually occur either in association with the Fe-Ti oxides or are included within them

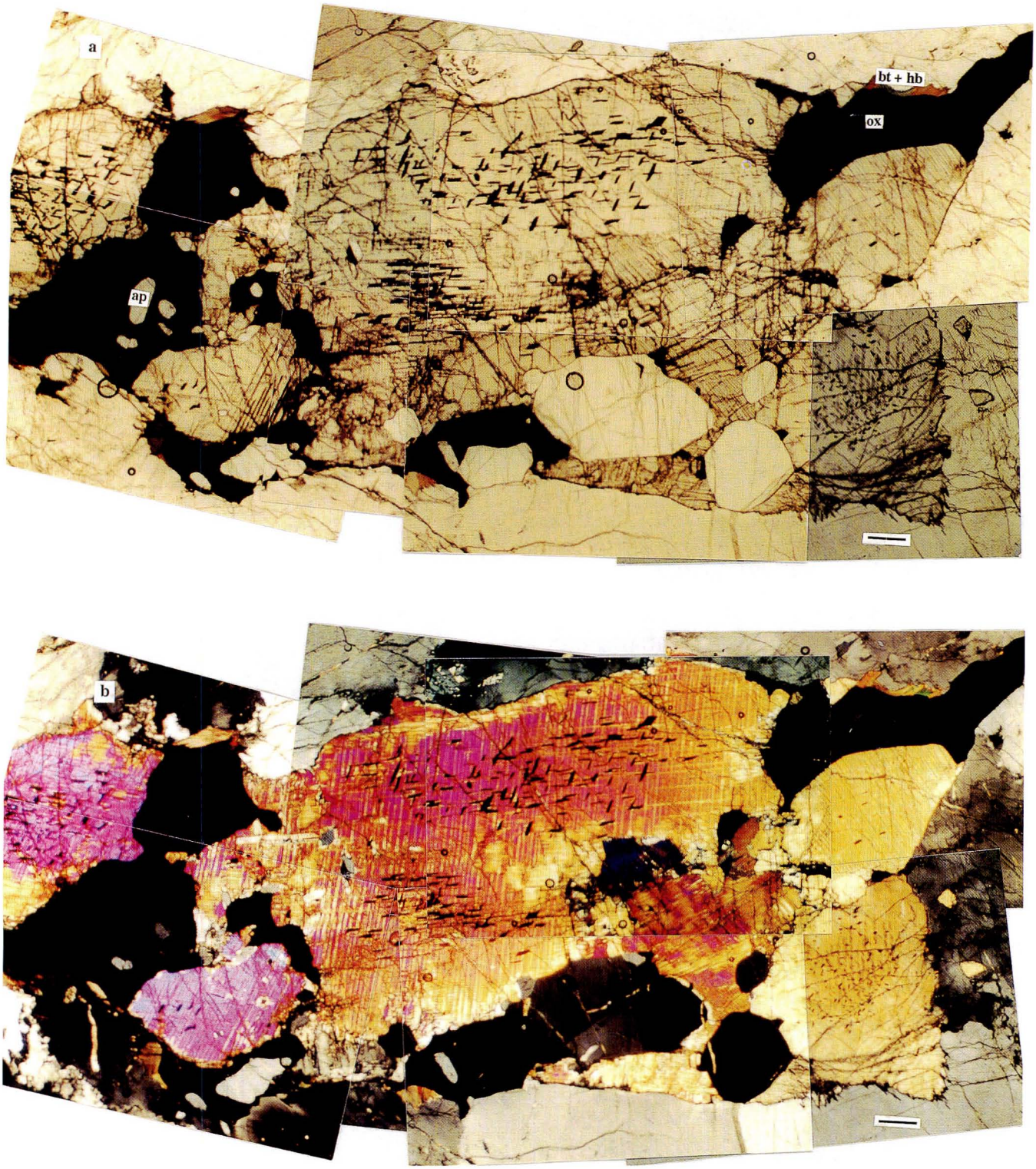

Fig. 4. Montage of photomicrographs of clinopyroxene phenocrysts illustrating the complex nature of exsolution lamellae preserved by the pyroxene grains. The thick and fine silicate lamellae are visible optically under high magnification and under crossed nicols. The invariable presence of oxide exsolution lamellae is also seen. The matrix is mostly plagioclase with little K-feldspar. ox-opaque oxide; ap-apatite. Bar scale is 0.1 mm.
a. open nicols b. crossed nicols

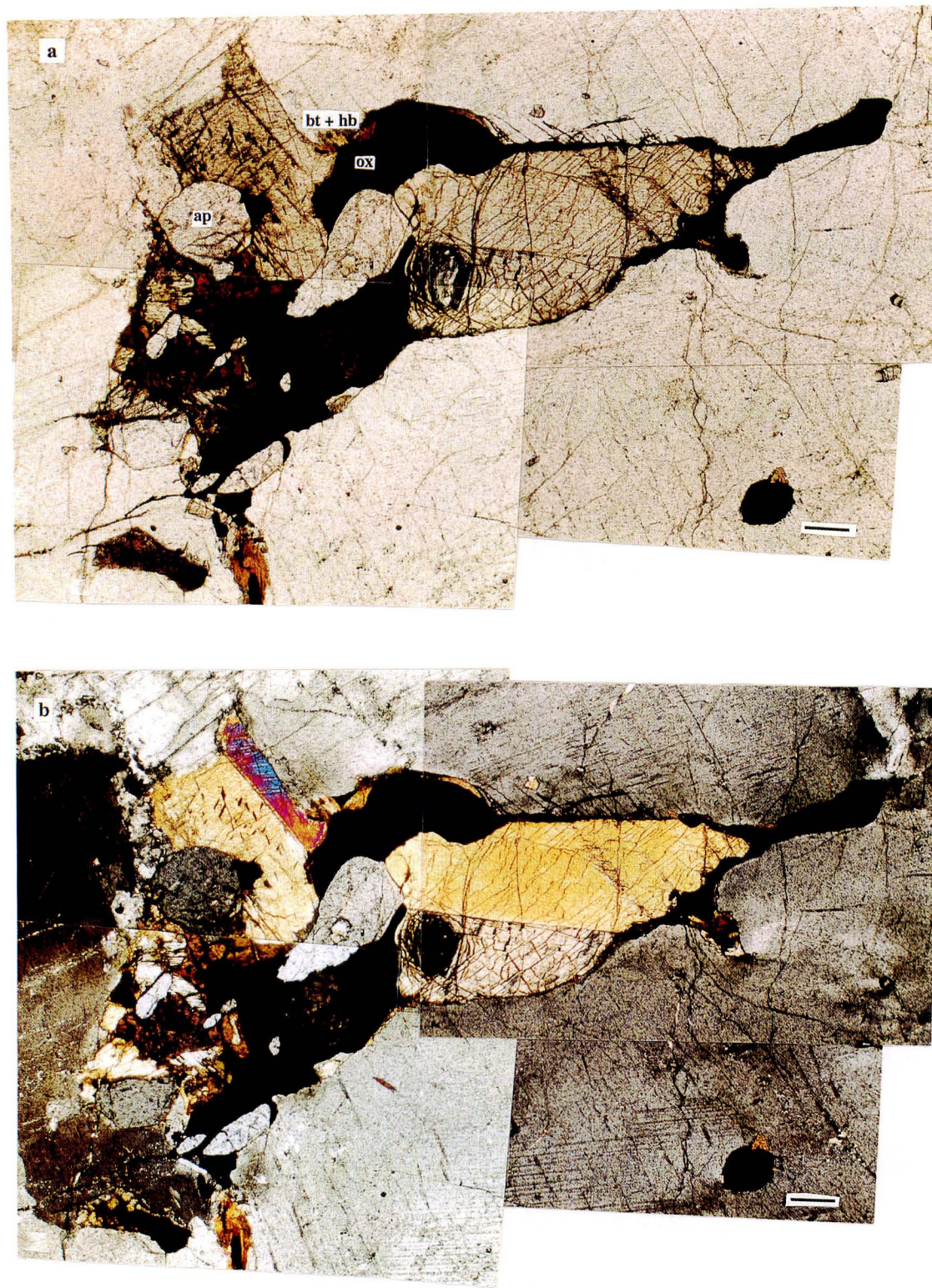

Fig. 5. Montage of photomicrographs of pyroxene phenocrysts showing exsolution. The two large grains on the top right and left of the photograph are clinopyroxene phenocrysts twinned on (100) and showing multiple exsolution lamellae (see also Plate 1.3). This constitutes the fine chevron exsolution lamellae of orthopyroxene in clinopyroxene, with the two twin individuals extinguishing in different positions. Oxide exsolution can also be seen. The grain on the bottom left of the photograph is a clinopyroxene phenocryst showing extensive orthopyroxene exsolution. The matrix is mostly plagioclase with little K-feldspar. ox - opaque oxide; ap - apatite. See text for details. Bar scale is 0.1 mm.
a. open nicols b. crossed nicols

(Figs. 4a, b, 5a & b), with occasional occurrence of aggregates of coarse apatite crystals. Locally apatite show abundant modal proportion (upto 6 per cent modal), especially in the norite samples. Red-brown biotite and green hornblende are present typically at the phenocryst margins. Inverted pigeonite, which forms an accessory constituent in most of the samples studied, is dot by biotite and hornblende grains.

The mafic and silicic minerals show varying degrees of alteration. Oriented inclusions are abundant in the interiors of pyroxene grains. In places, the host pyroxene does not have perfect extinction in cross-polarized light, presumably as a result of the numerous included sub micrometer lamellae of various sorts, but is otherwise optically normal. The color of the inclusion-bearing clinopyroxene is generally light green while orthopyroxene is light brown. The degree of exsolution features preserved in the anorthositic samples increase with increase in the mafic mineral content, with almost pure anorthosite samples exhibiting relatively little exsolution.

Study techniques

In order to determine the volume proportion of various exsolution features in the pyroxene phenocrysts, twelve grains were selected. Reflected light photomicrographs were taken at 6 - 8 areas, each approximately 150 μm by 100 μm, containing evenly distributed exsolution lamellae. The images were point-counted and converted into modal proportions. This will give a minimum estimate, as very small particles may not be resolved in an optical photomicrograph, but these probably contribute only a small additional volume of the exsolved phase.

Whole-rock XRD analysis was performed on powered rock samples using a Philips PW3020 diffractometer using Ni-filtered, CuKα radiation and a scanning speed of 1° min^{-1}.

Considering the fine and complex nature of most of the pyroxene exsolution features, we resorted to color imaging studies using energy dispersive X-ray (EDX) techniques on carbon-coated polished thin sections. Depending on the homogeneity of the exsolution pattern, the grains were partly or entirely covered by color imaging studies. Color imaging studies were performed on a computer controlled scanning electron microscope (SEM) Jeol JED-2000 at accelerating voltage - 15 kV and $5X10^{-8}$ A. After identification of the host pyroxene, the elements diagnostic of the exsolution phase were selected for color imaging such as Ca, Fe, Mg, Al and Ti.

General features of exsolution in pyroxene phenocrysts

Optically, the most obvious and striking feature of the anorthosite samples studied is the occurrence of various exsolution features in the pyroxenes (Figs. 4a, b, 5a & b). Both orthopyroxene and clinopyroxene occur most commonly as two separate phases, with occasional, closely intergrown subhedral grains; both exhibit numerous fine and coarse, closely and widely spaced exsolution lamellae that are only visible at high magnification and best under crossed nicols. The co-existence of orthopyroxene and clinopyroxene in all samples observed is marked by exsolution features involving orthopyroxene, augite and/or pigeonite. These exsolution features commonly occur both as isolated lamellae and as integral parts of composite lamellae with plagioclase and Fe-Ti oxide lamellae; but sometimes they show no obvious spatial relationship to these lamellae. Detailed optical and color imaging studies by EDX of these pyroxenes demonstrate that they display a complex mixture of several different types of lamellae.

The different types of exsolution lamellae observed include:

1. Plagioclase lamellae,
2. Orthopyroxene lamellae,
3. Clinopyroxene lamellae,
4. Fe-Ti oxide (magnetite, ilmenite, haematite and rutile) lamellae,
5. Biotite lamellae (?).

A common feature of these exsolution features is their straight and semi-parallel alignment. Although mostly incoherent, semi-coherent interface boundaries are frequent between the host and the exsolved phase (Williame and Brown, 1974; Buseck et al., 1980). Commonly, two types of exsolution lamellae are observed, one being mostly rather wide and the other being a thinner variety, which sometimes occurs in the complete absence of dislocations. The widths of exsolution lamellae vary from microscopic (micrometer size) to submicroscopic (nanometer size). Lamellar spacing is variable, with the distances between them being

less in the case of finer lamellae and more, and sometimes uniformly spaced, in the case of coarser lamellae. Most of these lamellae are not randomly distributed, but tend to be concentrated and evenly developed along imperfections, such as twin and low-angle grain boundaries in the host pyroxene; others may be related to sub-microscopic features such as twins and dislocations. They also occur as flattened, rod-shaped blebs in the host pyroxene. All phases in lamellae are crystallographically oriented in the pyroxene hosts and are essentially those of the planes of best fit at nucleation. Slight variations of orientation are often observed within a set of lamellae oriented in the same general direction. Although most of the orientations of these lamellae are not strictly parallel to the particular plane of the host, as illustrated by previous studies (e.g., Jaffe et al., 1975; Robinson et al., 1971; 1977), they are referred here as nearly parallel to that plane. The proportion, size, and spacing of the various exsolution lamellae in the host show slight variation from sample to sample and also between two pyroxene phenocrysts. In some instances, due to their narrow width, it was not always possible to distinguish optically (as well as using EDX techniques) the type of lamellae observed, and in such instances we resorted to comparative studies. These exsolution (or intergrowth) features are described here separately for both clinopyroxene and orthopyroxene phenocrysts. Matrix pyroxene is also characterized by the occurrence of exsolution features.

Clinopyroxene phenocrysts

Optically, the most striking and predominant exsolution phase in clinopyroxene phenocrysts is the plagioclase exsolution lamellae, although in some samples the proportion is less compared to the pyroxene exsolution. Commonly, two sets of plagioclase lamellae are observed, with the thicker lamellae, oriented nearly parallel to (100) of the host (Plate 1.1 & 1.2), being more common. The average volume proportion of the thick lamellae within a single clinopyroxene phenocryst is 30-45 per cent and the thin lamellae have a volume proportion of 30-38 per cent. Individual plagioclase lamellae have a relatively constant width (>10mm to 80 mm), with lamellae spacing being variable, the distances between thick closely spaced lamellae being more uniform (Plate 1.1 & 1.2) than thin, comparatively widely spaced lamellae. Most of the plagioclase lamellae span almost the entire length of the host clinopyroxene, but some are discontinuous. Extremely fine plagioclase lamellae have been observed in a clinopyroxene phenocryst, making an acute angle to the *c*-crystallographic axis of the host. Bulging of thick plagioclase exsolution lamellae as they approach each other was noticed in some samples (Plate 1.2).

Clinopyroxene phenocrysts, twinned on (100) and showing multiple exsolution lamellae of orthopyroxene, is a unique feature observed in most of the samples (Figs. 5a & b and Plate 1.3). The extensive nature of orthopyroxene exsolution was sometimes observed in clinopyroxene phenocrysts, presumably without any crystallographic orientation (average volume proportion within a single clinopyroxene phenocryst is 18-24 per cent) (Figs. 6&7). Clinopyroxene phenocrysts show exsolution (rather inversion) similar to inverted pigeonite structures, with the roles reversed, leading to features like diallage (also see Hatch et al., 1984) (Fig. 6 and Plate 1.4). Diallage is diagnostically marked by the characteristic bronzy sheen of the clinopyroxene. Clinopyroxene phenocrysts usually show both orthopyroxene and pigeonite exsolution. They usually contains two sets of orthopyroxene exsolution lamellae nearly parallel to the (100) plane, the most common one being represented by thick (10-35 μm), continuous/discontinuous lamellae (Fig. 8 and Plate 1.5); another set of comparatively fine (3-8 μm) exsolution lamellae constitute the less common one (Plate 1.6). A close look at the exsolution pattern in Plate 1.6 shows that the fine (100) lamellae have thicker and thinner varieties, with variable lamellae spacing (Plate 1.7 and Fig. 9). Some of the thicker (100) lamellae show bulging along their length (a hint of the texture is seen in Plate 1.7). The (100) lamellae occur both as isolated (continuous/-discontinuous) lamellae and as cutting the (001) pigeonite lamellae (Plate 1.8). The average volume proportion of the thick and fine lamellae within a clinopyroxene phenocryst is 15-22 per cent and 16-20 per cent, respectively. Some of the clinopyroxene phenocrysts show peculiar exsolution features of two sets of fine pigeonite lamellae, both making obtuse angles with the c-crystallographic axis of the host (average volume proportion within a single clinopyroxene phenocryst is

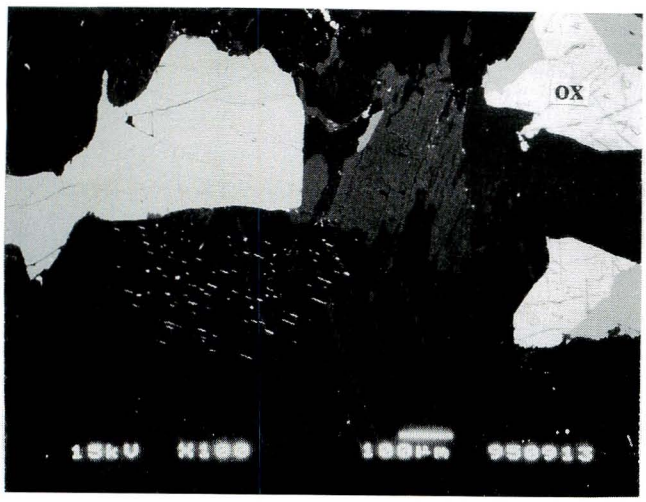

Fig. 6. Back-scattered Electron Imagery (BEI) of a clinopyroxene phenocryst showing exsolution lamellae of orthopyroxene which is rendered particularly conspicuous by the occurrence of hair-like rodlets of magnetite (white rodlets in the photograph), presumably formed from the latter. The grain to the left of this phenocryst is a clinopyroxene showing extensive orthopyroxene exsolution. Opaque oxide (ox) grains, which represent intergrowth of magnetite and ilmenite are also seen. See text for details.

18-24 per cent) (also see Robinson et al., 1971; 1977). The rare occurrence of three sets of pigeonite lamellae was observed in some samples, the most common one being parallel to (001) (coarse and uniformly spaced; mostly continuous) and (100)(fine and closely spaced; discontinuous), the other being nearly parallel to (001)(only visible under EDX) similar to those observed by Jaffe et al. (1975) and Rietmeijer and Champness (1982).

Orthopyroxene exsolution lamellae in clinopyroxene phenocrysts show constant association with Fe-Ti oxide lamellae, which are distributed more abundantly in the inner portions of the phenocryst (Plate 2.1). The average volume proportion of oxide inclusions within a clinopyroxene phenocryst is 2-8 per cent, this being a minimum estimate as very small particles may not be resolved in an optical photomicrograph. They usually occurs as rod-like, needle-like and/or plate-like particles constituting isolated lamellae, and also as integral parts of composite lamellae with plagioclase. They are restricted to interlamellar areas and align to form bands of inclusions. Color imaging studies by EDX reveal that most of the clinopyroxene phenocrysts contain dust-like much smaller oxide particles, in addition to the large particles. Magnetite constitutes the dominant oxide lamellae, although in some samples both magnetite and ilmenite constitute the dominant phase, with rutile being relatively less dominant. At least two lamellae orientations can be seen in a single host grain (Plate 2.1), with occasional occurrence of multiple orientations (in more than two directions) (Plate 2.2). Magnetite platelets occur in two orientations lying in the Z {slightly inclined to (100) plane of augite} and X {slightly inclined to (001) plane of augite} (also see Bown and Gay, 1959; Le Maitre, 1965; McCallum et al., 1975; Elsdon, 1971; 1972; Goode and Moore, 1975; Fleet et al., 1980) orientations of the host, with volume proportions of the former exceeding the latter in all the samples studied. Some of the clinopyroxene grains are dusted with fine magnetite platelets (Fig. 11). Ilmenite platelets commonly occur parallel to the (010) plane of the host, with a less common variety parallel to the (001) plane of the host also being observed. In some samples, especially those containing two sets of orthopyroxene lamellae, two types of ilmenite lamellae occur. One is nearly parallel to the (100) plane and the other slightly inclined to the (001) plane, and both are characterized by plate-like shapes (Plate 2.3). Rutile inclusions were less frequently observed in clinopyroxene phenocrysts, in comparison with orthopyroxene phenocrysts. They occur in four orientations, with variable lamellar width and lamellar spacing.

Orthopyroxene phenocrysts

Although less abundant compared to clinopyroxene phenocrysts, orthopyroxene phenocrysts have a wide and complex variety of exsolution and inversion features. They are in most respects similar, petrographically, to the clinopyroxene phenocrysts, in that they contain abundant plagioclase and Fe-Ti oxide lamellae. Orthopyroxene phenocrysts have additional lamellae of clinopyroxene. Like the clinopyroxene phenocrysts, the orthopyroxene phenocrysts also contain two sets of plagioclase exsolution lamellae, the most common being oriented parallel to (100) of the host, with one set of thin, exsolution lamellae and the second set of thick, exsolution lamellae (Plate 2.4), both having a relatively constant width. The thicker lamellae are sometimes discontinuous and show slight thickening and thinning along their

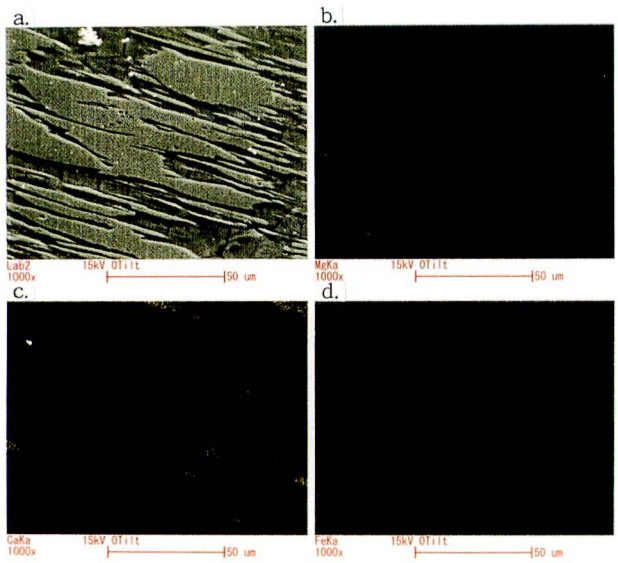

Fig. 7. Color images of Mg, Ca and Fe distribution in a clinopyroxene phenocryst using Energy Dispersive X-ray (EDX) techniques to illustrate the extensive nature of orthopyroxene exsolution.
a. compositional image, b. characteristic X-ray image of MgKα, c. characteristic X-ray image of CaKα, d. characteristic X-ray image of Fe Kα.

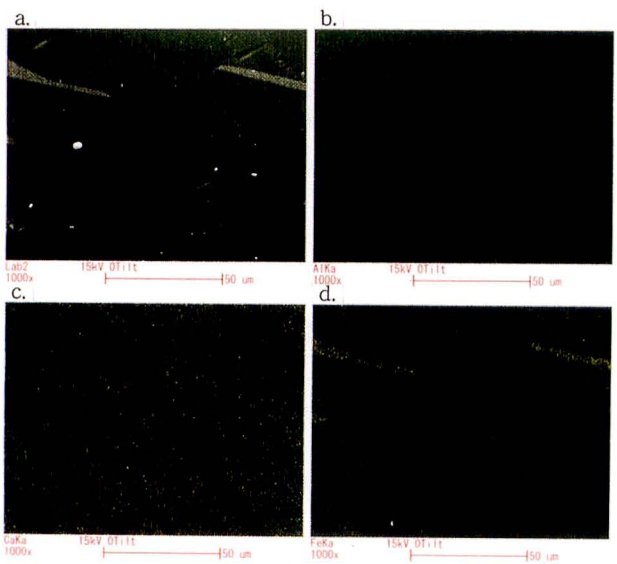

Fig. 9. Color images of Al, Ca and Fe distribution in a clinopyroxene phenocryst using EDX techniques, to illustrate two sets of fine orthopyroxene exsolution lamellae (one continuous and other discontinuous). Oxide (magnetite) lamellae can also be seen.
a. compositional image, b. characteristic X-ray image of AlKα, c. characteristic X-ray image of CaKα, d. characteristic X-ray image of Fe Kα.

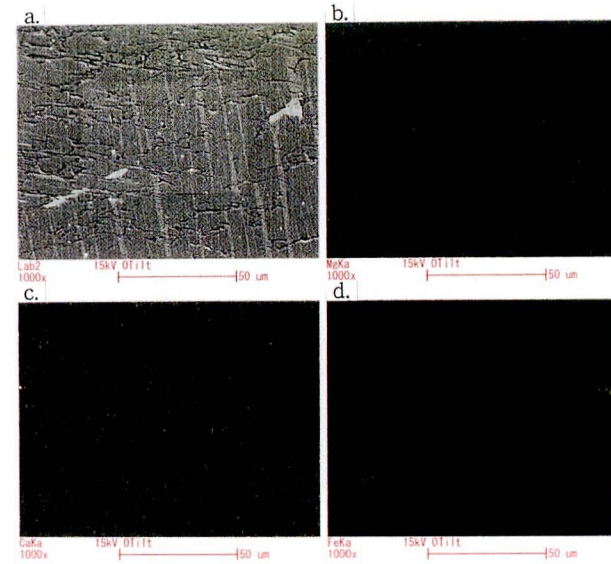

Fig. 8. Color images of Mg, Ca and Fe distribution in a clinopyroxene phenocryst using EDX techniques to illustrate thick and thin varieties of orthopyroxene lamellae nearly parallel to the (100) plane. The lamellae are mostly discontinuous and appear like an elongated eye tapering towards the ends within the host, although continuous varieties constitute the dominant (100) orthopyroxene exsolution in clinopyroxene phenocrysts. Oxide (magnetite) lamellae can also be seen.
a. compositional image, b. characteristic X-ray image of MgKα, c. characteristic X-ray image of CaKα, d. characteristic X-ray image of Fe Kα.

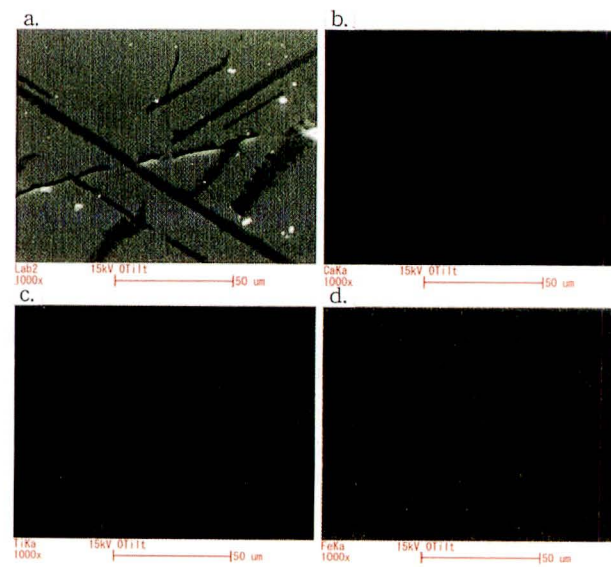

Fig. 10. Color images of Ca, Ti and Fe distribution in a orthopyroxene phenocryst using EDX techniques, to illustrate four directions of rutile exsolution lamellae.
a. compositional image, b. characteristic X-ray image of CaKα, c. characteristic X-ray image of TiKα, d. characteristic X-ray image of Fe Kα.

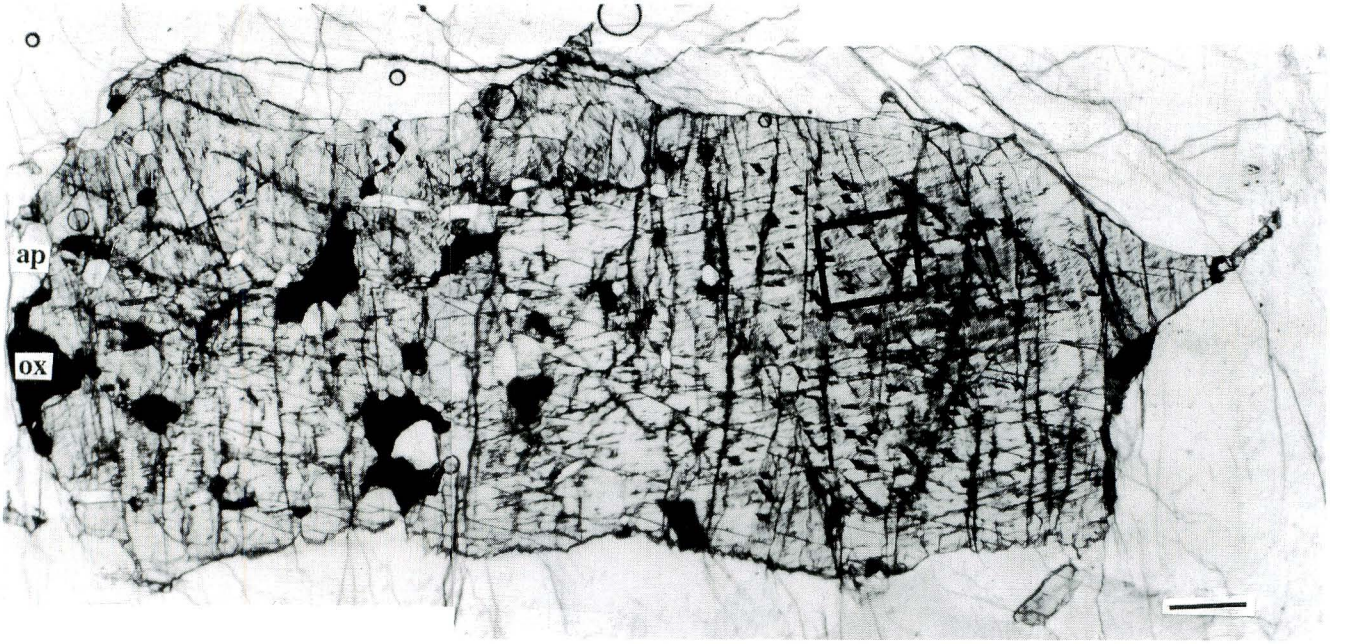

Fig. 11. Montage of two photomicrographs of a clinopyroxene phenocryst showing the "dusty" oxide exsolution. ox - opaque oxide; ap - apatite. Bar scale is 0.1 mm. (open nicols)

lengths (Plate 2.5). The average volume proportions of the thin and thick exsolution lamellae within a single orthopyroxene phenocryst are 20-25 per cent and 18-24 per cent respectively. Close observation of these plagioclase lamellae reveals that some of them are, in fact, discontinuous, containing segments of Fe-Ti oxide (ilmenite or magnetite) similar to the so-called combination lamellae quoted by many authors (e.g., Veblen and Bish, 1988) (Plate 2.6). Larger lamellae of plagioclase were observed to be surrounded by precipitate-free zones, devoid of narrow lamellae, with some of them showing association with biotite, constituting a probable minor exsolution phase (?).

Clinopyroxene exsolution constitutes a significant phase in orthopyroxene phenocrysts as both blebby exsolution (Fig. 12 and Plate 2.7) and lamellar exsolution, the latter being far more dominant. The blebs are irregular in shape and have a common elongation direction and almost similar optical orientation. They usually form subparallel trails at high angles to fine exsolution lamellae of clinopyroxene, and exhibit no consistent cross-cutting relationship with the latter. Orthopyroxene phenocrysts contain three sets of clinopyroxene exsolution lamellae (although they rarely occur together), the most common one being represented by fine to very fine (3-10 μm), numerous and closely spaced lamellae nearly parallel to the (100) plane (Plate 2.8). The average volume proportion of the lamellae within a single orthopyroxene phenocryst is 17-22 per cent. These lamellae are sometimes thickened by the propagation of ledges along the (100) interface (Plate 3.1 & 3.2), similar to those observed by Champness and Lorimer (1973) and Kohlstedt and Vander Sande (1976). In contrast to the fine augite lamellae, some of the orthopyroxene phenocrysts show one set of thick clinopyroxene lamellae nearly parallel to the (100) plane. Some of the orthopyroxene phenocrysts show one set of evenly spaced, uniformly thick (comparatively) (15 - 30 μm) and inclined exsolution lamellae of augite parallel to (001), which are characterized by their equal thickness and uniform distribution (Plate 3.3). The average volume proportion of the lamellae within a single orthopyroxene phenocryst is 14-18 per cent. In some samples the presence of a smaller set of very fine exsolution lamellae was observed within these broad exsolution lamellae of clinopyroxene, similar to that described by Boyd and Brown (1969) from a Bushveld inverted pigeonite. Some of the orthopyroxene phenocrysts show peculiar patterns of exsolution (rather inversion) lamellae, leading to features like inverted pigeonite (Plate 3.4) (also see Poldervaart and Hess, 1951; Brown, 1957; 1972; Ishii and Takeda, 1974; Smith,

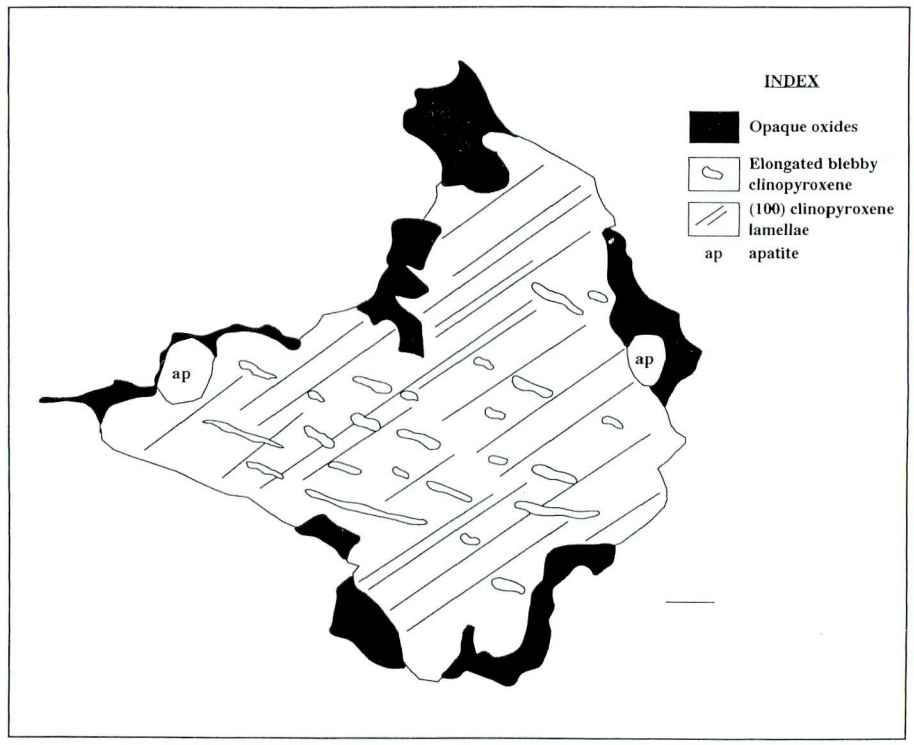

Fig. 12. A sketch of an orthopyroxene phenocryst showing blebby exsolution of irregular shaped, elongated optically oriented clinopyroxene. Bar scale is 0.01 mm.

1974; Morimoto and Tokonami, 1969; McKenzie and Guilford, 1986) and herringbone or chevron type of exsolution (also see Cox et al., 1979; Philpotts, 1989). Although rare, some of the orthopyroxene phenocrysts contain three sets of clinopyroxene exsolution lamellae: one set represented by prominently oriented continuous lamellae (20 - 25 μm) parallel to (100) of the host; a second set of fine, discontinuous lamellae (13 - 15 μm) almost parallel to (001); and the third set of very fine lamellae (6 - 10 μm) (mostly visible only under EDX), making an acute angle to the c-crystallographic axis.

Fe-Ti oxides constitute the next significant exsolution phase in orthopyroxene phenocrysts, occurring as platelets and rodlets of ilmenite (with occasional intergrowth with haematite: hemoilmenite), magnetite or rutile, upto a few tens of microns in width. The average minimum volume proportion of oxide inclusions within a orthopyroxene phenocryst is 5-10 per cent. As in clinopyroxene phenocrysts, they are distributed abundantly in the inner portions of the orthopyroxene phenocrysts rather than in the margins. Ilmenite lamellae constitute the most abundant Fe-Ti oxide exsolution phase (Plate 3.5), followed by magnetite, although in some samples they occur in equal proportions. Two orientations of very fine needle to plate-like lamellae of ilmenite parallel to the (010) and (001) planes have been observed, with rare occurrences of ilmenite lamellae in one direction (Plate 3.6). Ilmenite lamellae are typically elongated compared to the magnetite lamellae (Plate 3.6 & 3.7). The largest ilmenite particles that can be observed by EDX color imaging retain the approximate lattice relation to the host, but they lack the platy morphology of the small particles. Magnetite occurs usually as rods lying in the (100) plane (Z plane of orthopyroxene) and are similar in appearance and distribution to the Z inclusions in augite (also see Fleet et al., 1980). A second set of magnetite lamellae, probably occurring normal to (111), as demanded by the intergrowth symmetry principle, is also seen in orthopyroxene phenocrysts. Rutile inclusions occur in four orientations, the most common being usually elongate along the c-axis, and the bulk of them falling in the optically unresolvable range as an oxide phase (Fig. 10). All orientations can be found close together, but there is a tendency for one of them to predominate within areas of a size approximately 100 μm^2.

Matrix pyroxene

Matrix pyroxene grains invariably exhibit rare, fine, plagioclase exsolutions. Matrix clinopyroxene grains rarely exhibit orthopyroxene exsolution lamellae, although some grains clearly show thin lamellae of orthopyroxene. Matrix orthopyroxene grains sometimes contain fine, uniformly spaced (continuous/discontinuous) clinopyroxene exsolution lamellae, although many are clinopyroxene-lamellae free. Nearly all the matrix pyroxene grains contain thin, exsolved platelets of oxide phases (Plate 3.8) (either ilmenite or magnetite in all the grains examined - we are not ruling out the possibility of very fine rutile or other oxide lamellae, too fine to be detected).

Discussion-evidence for progressive exsolution

The present study clearly illustrates the complex nature of exsolution features preserved in pyroxene phenocrysts, further substantiating the recent concept that these pyroxenes are microstructurally far more complex than the pyroxenes from basalts and gabbros that have been exten sively characterized(e.g., Buseck et al., 1980; Veblen, 1985; Veblen and Bish, 1988). In most of the samples studied, there was enough evidence for progressive or continual exsolution during slow cooling of the pyroxene grains. Various studies on pyroxene megacrysts from massif-type anorthosite occurrences have suggested that the diversity of exsolution products is a testament to the enhanced incorporation of both nonquadrilateral and non-pyroxene components into the growing pyroxene crystals (Dymek and Gromet, 1984; Veblen and Bish, 1988; Owens and Dymek, 1995). The orientations of various exsolution lamellae are essentially those of the planes of best fit at nucleation, and can be compared to observed and theoretically calculated orientations of similar intergrowths reported by previous studies. Thicker scale exsolution textures, like those in Plate 1.1 and 2.4, generally consist of lamellae with nearly planar interfaces, while thinner scale textures show some deviation from planar morphology. Strain-field interactions have been suggested by Livi and Veblen (1989) as being partially responsible for the unusual lamellar morphologies, especially the bulging of lamellae as they approach each other. The presence of precipitate-free zones near plagioclase lamellae could result from solute depletion in this zone, if the lamellae formed early (Veblen and Bish, 1988).

It follows from previous experimental studies focusing on mechanism of exsolution (e.g., Boyd and Schairer, 1964; Kushiro, 1972; McCallister and Yund, 1977) that rapid exsolution kinetics resulting in the development of the modulated microstructure (characterized by fine-scale irregular lamellae) indicate spinodal decomposition as result of rapid cooling and the consequent high supersaturation (Cahn, 1968; Champness and Lorimer, 1971; 1976), while the more regular microstructure (characterized by regular wider-spaced lamellae) suggests the possibility of coherent nucleation and growth as a mechanism (Copley et al., 1974). Pyroxenes probably constitute one of the best known multicomponent systems in mineralogy and also provide us with perhaps the best record of coherent exsolution of all mineral systems (Robin and Ball, 1988). Buseck et al., (1980) examines the mechanisms of exsolution possible in pyroxenes in detail (Fig. 13). From Fig. 13, it follows that the continuous free-energy curves between pigeonite and augite points towards a possible exsolution by spinodal decomposition as well as by nucleation and growth, while discontinuous free-energy curves between orthopyroxene and augite rules out the possibility of spinodal decomposition as a possible mechanism of exsolution for this pair (Buseck et al., 1980). Whereas in nucleation a distinct interface is present at the onset of exsolution, in spinodal decomposition exsolution proceeds by the development of a compositional modulation (cf. Buseck et al., 1980).

Regarding various silicate lamellae, the overall spatial distribution, especially in areas where there were no dislocations, and the apparent consideration of orientation relation on inclusion attitude, are consistent with slow cooling of the pyroxene, resulting in coherent exsolution by heterogeneous precipitation and growth of the new lamellae (Nord et al., 1975; Ross and Huebner, 1979; Buseck et al., 1980). The semicoherent nature of the interface boundaries in the case of pyroxene exsolution, together with the ledges identified in some of these pyroxene interfaces, supports nucleation and growth as the possible mechanism of exsolution (Champness and Lorimer, 1974; Copley et al., 1974; Kohlstedt and Vander Sande, 1976; Ross and Huebner, 1979; Buseck et al., 1980). The style of

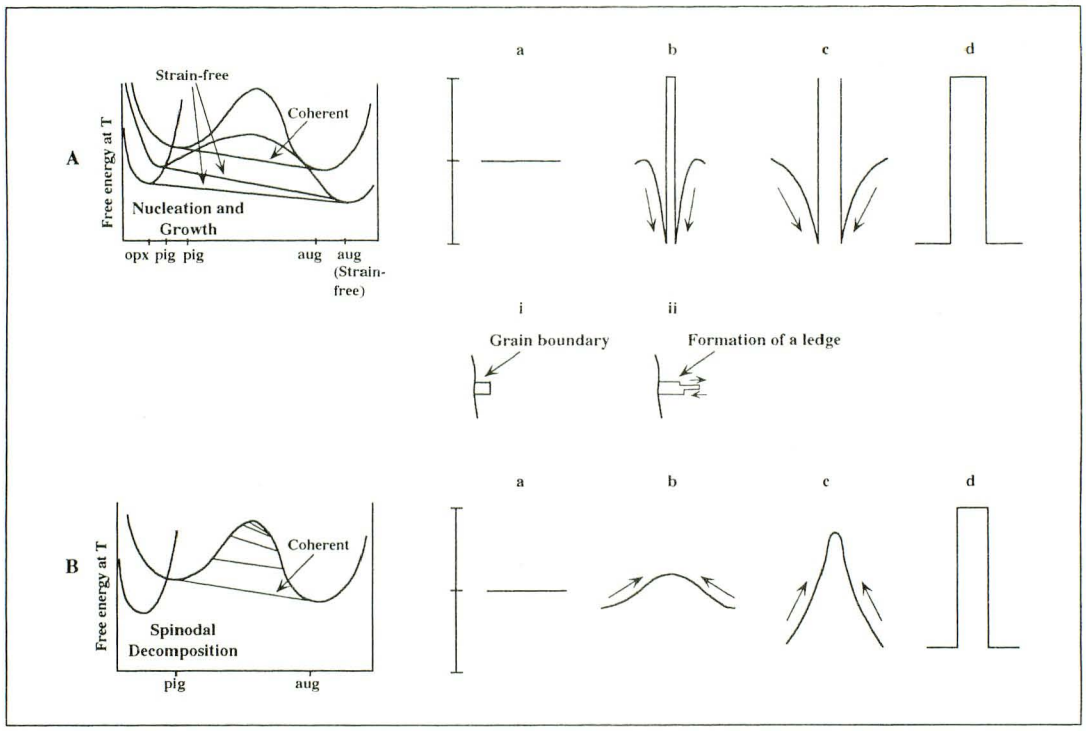

Fig. 13. Schematic diagrams (free-energy versus composition diagram; temperature versus composition diagram; cartoons illustrating the formation of intergrowth) illustrating the exsolution (intergrowth) mechanisms of
A. nucleation and growth, where an unstable solid could decompose by forming compositional fluctuations that are large in magnitude and small in extent
B. spinodal composition, where an unstable solid could decompose by forming compositional fluctuations that are large in extent and small in magnitude
The formation of an intergrowth by both these mechanisms is illustrated from their original state (a), with gradual change in composition (b & c) to the final state (d) of intergrowth texture. Spinodal decomposition involves so-called 'uphill' diffusion, while nucleation and growth involves 'downhill' diffusion with steeper gradients. Considering the observation of thickening of lamellae by propagation of ledges, heterogeneous nucleation of a precipitate at grain boundary (i) together with formation of ledges (ii) assumes significance. pig-pigeonite, opx-orthopyroxene, aug-augite (cf. Copley et al., 1974; Buseck et al., 1980; Putnis and McConnell, 1980; Shelley, 1993). See text for details.

exsolution that is normally ascribed to spinodal decomposition (fine, wavy intergrowths) (Cahn, 1968), which forms the prefect alternative for nucleation and growth mechanism, was not observed in the pyroxene phenocrysts of the present study.

The oxide platelets are commonly more abundant in inner portions of the pyroxene phenocrysts and depleted near the margin, perhaps suggesting collectively the outline of the original cumulus grains. In principle, such a particle distribution, free from interfering effects of irreproducible heterogeneities, is amenable to the application of the kinetic theory of nucleation and growth (Yund and McCallister, 1970). The scenario proposed is that the various silicate lamellae particles might have nucleated heterogeneously, while the smaller precipitates (oxide lamellae) are interpreted as a homogeneously nucleated analogue of the first. The homogeneous exsolution phenomenon is particularly interesting as a potential indicator of the history of cooling through a range of high temperatures.

The differing orientations of several generations of pigeonite exsolution lamellae identified in clinopyroxene phenocrysts reflect the changes in the plane of minimum-misfit at their nucleation temperatures (Robinson et al., 1971; 1977). The rigorous orientation of oxide lamellae in pyroxene phenocrysts, with planes of oxygens that are in closest packing or positions near those of closest packing being parallel to respective pyroxene orientations, illustrates the topotactic control of intergrowth orientation, probably resulting from the shared structural elements between the lamellae and host (Fleet and Arima, 1985). The Z and X magnetite inclusions are, respectively, equivalent

to (100) and (001) exsolved pigeonite lamellae in augite (Fleet et al., 1980).

The composition and occurrence of Fe-Ti oxides in igneous rocks is not only a function of the composition of the melt from which the oxides crystallized, but is also determined by reactions between the oxides and the silicates in the rock (Osborn, 1962; Carmichael, 1967; Frost et al., 1988; Lindsley et al., 1990: Frost and Lindsley, 1991). Evaluating the occurrence of Fe-Ti oxide phases in deep-seated rocks, Barink (1982) illustrated that silicates crystallized at high temperatures may be nonstochiometric, and the oxygen released upon cooling may combine with Fe^{2+} and Ti to produce magnetite or ilmenite inclusions in the host phase. The occurrence of discontinuous lamellae of plagioclase containing segments of Fe-Ti oxide in orthopyroxene phenocrysts suggests that plagioclase and Fe-Ti oxide formed concurrently by precipitation (exsolution) from the orthopyroxene host. The occurrence of exsolved platelets of Fe-Ti oxide (magnetite) in these orthopyroxene phenocrysts is in contention with Morse's (1975) recognition that plagioclase exsolution from orthopyroxene requires a source of silica, which is provided by the oxidation of the $FeSiO_3$ component in orthopyroxene. This is illustrated by the following two-stage reaction of:

(1) $3FeSiO_3 + 1/2O_2 = Fe_3O_4 + 3SiO_2$

(2a) $CaAl_2SiO_6 + SiO_2 = CaAlSi_2O_8$

(2b) $NaAlSi_2O_6 + SiO_2 = NaAlSi_3O_8$

(cf. Morse, 1975).

The involvement of magnetite in the exsolution with plagioclase is in rough accordance with the two possible isochemical exsolution reactions of:

(1) $3CaAlSi_2O_8 + Fe_3O_4$
$= 3CaAl_2SiO_6 + 3FeSiO_3 + 1/2O_2$

(2) $6NaAlSi_3O_8 + 3Fe_3O_4$
$= 3FeAl_2SiO_6 + 6NaFeSi_2O_6 + 3FeSiO_3 + 1/2O_2$

(cf. Emslie, 1975; Bohlen and Essene, 1978).

The presence of biotite as a probable exsolution (?) phase associated with plagioclase lamellae, presumably forms as a result of unmixing of K from the host pyroxene (Morse, 1975; Veblen and Bish, 1988).

The occurrence of features like diallage may presumably, be a direct consequence of the change in composition of augites with falling temperatures. Similarly, the occurrence of three generations of pigeonite exsolution lamellae in augite, and other typical exsolution and inversion features like inverted pigeonite, herring-bone or chevron type, are indicative of a high initial crystallization temperature and also a high degree of cooling for the anorthosite (Robinson et al., 1977).

The occurrence of co-existing pyroxenes, each of which displays exsolution features, is a diagnostic feature of tholeiitic intrusions, and contrasts with the single pyroxene trend, lacking exsolution, of alkali basic intrusions. The occurrence of inverted pigeonite and Fe-rich orthopyroxene typically characterizes the host rocks as subalkaline. The presence of high temperature mineralogy and anhydrous mineral assemblages suggest that the magmas that characterize the parent magmas was dry. The association of oxide inclusions with pyroxene phenocrysts is noteworthy, and suggests that oxidizing conditions played an important role in controlling the properties and compositions of these phenocrysts. The exsolution features preserved in pyroxene phenocrysts from the Perinthatta anorthosite massif offer excellent opportunities to probe their crystallization histories.

Acknowledgments

We acknowledge the constructive comments of Prof. M. Itoh, Nagoya University, Japan, and, Dr. Y.J. Bhaskar Rao, NGRI, India, which helped in improving the presentation of the manuscript. The first author thanks Drs. Y. Osanai and T. Ueno of Fukuoka University of Education, Japan, for their hospitality and analytical assistance during his stay there. The first author thanks the Ministry of Education, Science and Culture (MONBUSHO), Japan, for a fellowship support. This is a contribution to the MONBUSHO International Research Project (Grant-in-Aid, International Scientific Research of Monbusho, No. 08041109), as well as to IGCP-368 and Gondwana Research Group.

References

Barink, H.W. (1982) Decrease in cation-deficiency in rock-forming minerals as the cause of the retrogressive oxidation of accessory Fe-Ti oxides in deep seated rocks: A new approach. *Neues Jahrbuch fur Mineralogie Monatsheft.*, 29-44.

Bohlen, S.R. and Essene, E.J. (1978) Igneous pyroxenes from metamorphosed anorthosite massifs. *Contrib. Mineral. Petrol.*, **65**, 433-442.

Bown, M.G. and Gay, P. (1959) The identification

of oriented inclusions in pyroxene crystals. *Amer. Miner.*, **44**, 592-602.

Boyd, F.R. and Brown, G.M. (1969) Electron-probe study of pyroxene exsolution. *Mineral. Soc. Amer. Sp. Pap.*, **2**, 211-216.

Boyd, F.R. and Schairer, J.F. (1964) The system $MgSiO_3$-$CaMgSi_2O_6$. *Jour. Petrol.*, **5**, 275-309.

Buseck, P.R., Nord, G.L., Jr., and Veblen, D.R. (1980) Subsolidus phenomena in pyroxenes. *Mineral. Soc. Amer. Rev. Minerals*, **7**, 117-211.

Cahn, J.W. (1968) Spinodal decomposition. *Trans. AIME*, **242**, 166-180.

Carmichael, I.S.E. (1967) The iron-titanium oxides of salic volcanic rocks and their associated ferromagnesian silicates. *Contrib. Mineral. Petrol.*, **14**, 36-64.

Champness, P.E. and Lorimer, G.W. (1971) An electron microscopic study of a lunar pyroxene. *Contrib. Miner. Petrol.*, **33**, 171-183.

Champness, P.E. and Lorimer, G.W. (1973) Precipitation (exsolution) in an orthopyroxene. *Jour. Materials. Sci.*, **8**, 467-474.

Champness, P.E. and Lorimer, G.W. (1974) A direct lattice-resolution study of precipitation (exsolution) in orthopyroxene. *Phil. Mag.*, **30**, 357-366.

Champness, P.E. and Lorimer, G.W. (1976) Exsolution in silicates. In Wenk, H.R. (ed.) Electron Microscopy in Mineralogy, *Springer-Verlag*, New York, 174-204.

Copley, P.A., Champness, P.E. and Lorimer, G.W. (1974) Electron petrography of exsolution textures in an iron-rich clinopyroxene. *Jour. Petrol.*, **15**, 41-57.

Cox, K.G., Bell, J.D. and Pankhurst, R.J. (1979) The Interpretation of Igneous rocks. *George Allen and Unwin*, London, 450.

Dymek, R.F. and Gromet, L.P. (1984) Nature and origin of orthopyroxene megacrysts from the St-Urban anorthosite massif, Quebec. *Cana. Miner.*, **22**, 297-326.

Elsdon, R. (1971) Clinopyroxenes from the Upper Layered Series, Kap Edvard Holm, East Greenland. *Miner. Mag.*, **38**, 49-57.

Elsdon, R. (1972) Iron-titanium oxide minerals in the Upper Layered Series, Kap Edvard Holm, East Greenland. *Miner. Mag.*, **38**, 946-956.

Emslie, R.F. (1975) Pyroxene megacrysts from anorthositic rocks: New clues to the sources and evolution of the parent magmas. *Cana. Miner.*, **13**, 138-145.

Fleet, M.E. and Arima, M. (1985) Oriented hematite inclusions in sillimanite. *Amer. Miner.*, **70**, 1232-1237.

Fleet, M.E., Bilcox, G.A. and Barnett, R.L. (1980) Oriented magnetite inclusions in pyroxenes from the Grenville Province. *Cana. Miner.*, **18**, 89-99.

Frost, B.R. and Lindsley, D.H. (1991) Occurrence of Iron-titanium oxides in igneous rocks. In: Lindsley, D.H. (ed.), Oxide Minerals, *Min. Soc. Amer. Rev. Miner.*, **25**, 433-468.

Frost, B.R., Lindsley, D.H. and Anderson, D.J. (1988) Fe-Ti oxide-silicate equilibria: Assemblages with fayalitic olivine. *Amer. Miner.*, **73**, 727-740.

Geological Survey of India (1995) Geological and Mineral map of Kerala on the scale 1:500,000. published by *GSI*, India.

Goode, A.D.T. and Moore, A.C. (1975) High pressure crystallization of the Ewarara, Kalka and Goose Pile intrusions, Giles complex, central Australia. *Contrib. Mineral. Petrol.*, **51**, 77-97.

Hatch, F.H., Wells, A.K. and Wells, M.K. (1984) Petrology of the Igneous rocks. *CBS Publishers*, Delhi, 551.

Ishii, T. and Takeda, H. (1974) Inversion, decomposition and exsolution phenomena of terrestrial and extraterrestrial pigeonites. *Geol. Soc. Japan, Mem.*, **11**, 19-36.

Jaffe, H.W., Robinson, P., Tracy, R.J. and Ross, M. (1975) Orientation of pigeonite lamellae in metamorphic augite: correlation with composition and calculated optimal phase boundaries. *Amer. Miner.*, **60**, 9-28.

Kohlstedt, D.L. and Vander Sande, J.B. (1976) On the detailed structure of ledges in an augite-enstatite interface. In Wenk, H.R. (ed.) Electron Microscopy in Mineralogy, *Springer-Verlag*, New York, 234-237.

Kushiro, I. (1972) Determination of liquidus relations in synthetic silicate systems with electron probe analysis: the system forsterite-diopside-silica at 1 atmosphere. *Amer. Miner.*, **57**, 1260-1271.

Le Maitre, R.W. (1965) The significance of the gabbroic xenoliths from Gough Island, South Atlantic. *Miner. Mag.*, **34**, 303-317.

Lindsley, D.H., Frost, B.R., Anderson, D.J. and Davidson, P.M. (1990) Fe-Ti oxide-silicate equilibria: Assemblages with orthopyroxene. In: Spencer, R.J. and Chou, I,-M, (eds.), Fluid-Mineral

Interactions: A tribute to H.P. Eugster, *The Geochemical Society, Special Publication No.2.*

Livi, K.J.T. and Veblen, D.R. (1989) Transmission electron microscopy of interfaces and defects in intergrown pyroxenes. *Amer. Miner.*, **74**, 1070-1083.

MacKenzie, W.S. and Guilford, C. (1986) Atlas of Rock forming minerals in thin sections. *ELBS/Longman*, Essex, England, 98.

McCallister, R.H. and Yund, R.A. (1977) Coherent exsolution in Fe-free pyroxenes. *Amer. Miner.*, 62, 721-726.

McCallum, I.S., Okamura, F.P. and Ghose, S. (1975) Mineralogy and petrology of sample 67075 and the origin of lunar anorthosites. *Earth Planet. Sci. Lett.*, **26**, 36-53.

Morimoto, N. and Tokonami, M. (1969) Oriented exsolution of augite in pigeonite. *Amer. Miner.*, **54**, 1101-1117.

Morse, S.A. (1975) Plagioclase lamellae in hypersthene, Tikkoatokhakh Bay, Labrador. *Earth Planet. Sci. Lett.*, **26**, 331-336.

Nord, G.L., Jr., Heuer, A.H., Lally, J.S. and Christie, J.M. (1975) Substructures in lunar clinopyroxenes as petrologic indicators. *Lunar Sci.* VI, 601-603.

Osborn, E.F. (1962) Reaction series for subalkaline igneous rocks based on different oxygen pressure conditions. *Amer. Miner.*, **47**, 211-226.

Owens, B.E. and Dymek, R.F. (1995) Significance of pyroxene megacrysts for massif anorthosite petrogenesis: Constraints from the Labrieville, Quebec, pluton. *Amer. Miner.*, **80**, 144-161.

Philpotts, A.R. (1989) Petrography of Igneous and Metamorphic rocks. *Prentice Hall*, New Jersey, 178.

Poldervaart, A. and Hess, H.H. (1951) Pyroxenes in the crystallization of basaltic magmas. *Jour. Geol.*, **59**, 472-489.

Putnis, A. and McConnell, J.D.C. (1980) Principles of Mineral Behaviour. *Blackwell*, Oxford, 257.

Rietmeijer, F.M.J. and Champness, P.E. (1982) Exsolution structures in calcic pyroxenes from the Bjerkreim-Sokndal lopolith, SW Norway. *Miner. Mag.*, **45**, 11-24.

Robinson, P., Jaffe, H.W., Ross, M. and Klein, C., Jr. (1971) Orientation of exsolution lamellae in clinopyroxenes and clinoamphiboles: consideration of optimal phase boundaries. *Amer. Miner.*, **56**, 909-939.

Robinson, P., Ross, M., Nord, G.L., Jr., Smyth, J.R. and Jaffe, H.W. (1977) Exsolution lamellae in augite and pigeonite: fossil indicators of lattice parameters at high temperature and pressure. *Amer. Miner.*, **62**, 857-873.

Ross, M. and Huebner, J.S. (1979) Temperature-composition relationships between naturally occurring augite, pigeonite and orthopyroxene at one bar pressure. *Amer. Miner.*, **64**, 1133-1155.

Shelley, D. (1993) Igneous and Metamorphic rocks under the microscope: Classification, textures, microstructures and mineral preferred orientations. *Chapman & Hall*, London, 445.

Smith, D. (1974) Pyroxene-olivine-quartz assemblages in rocks associated with the Nain anorthosite massif, Labrador. *Jour. Petrol.*, **15**, 58-78.

Streckeisen, A.L. (1976) To each plutonic rock its proper name. *Earth Planet. Sci. Rev.*, **12**, 1-33.

Veblen, D.R. (1985) Direct TEM imaging of complex structures and defects in silicates. *Ann. Rev. Ear. Planet. Sci.*, **13**, 119-146.

Veblen, D.R. and Bish, D.L. (1988) TEM and X-ray study of orthopyroxene megacrysts: Microstructures and crystal chemistry. *Amer. Miner.*, **73**, 677-691.

Vidyadharan, K.T., Sukumaran, P.V. and Nair, M.M. (1976) A note on the occurrence of anorthosite near Perinthatta, Taliparamba taluk, Cannanore district, Kerala. *Jour. Geol. Soc. India*, **118**, 117-130.

Williame, C. and Brown, W.L. (1974) A coherent elastic model for the determination of orientation of exsolution boundaries: application to feldspars. *Acta Crystallogr.*, **A30**, 316-331.

Yund, R.A. and McCallister, R.H. (1970) Kinetics and mechanisms of exsolution. *Chem. Geol.*, **6**, 5-30.

Plate 1

Plate 1.1. Photomicrograph of a clinopyroxene phenocryst showing plagioclase exsolution parallel to (100) of the host. Note the relatively constant width and nearly uniform lamellar spacing. Minor oxide platelets can also be seen at the bottom right of the photograph. Bar scale is 0.01 mm. (crossed nicols)

Plate 1.2. Photomicrograph of a clinopyroxene phenocryst showing plagioclase exsolution parallel to (100) of the host. Note bulging of thick plagioclase exsolution lamellae at the top right of the photograph. Bar scale is 0.03 mm. (crossed nicols)

Plate 1.3. Photomicrograph of a clinopyroxene phenocryst twinned on (100) and showing multiple orthopyroxene exsolution lamellae. This constitutes the fine, chevron exsolution lamellae of orthopyroxene in clinopyroxene, with the two twin individuals extinguishing in different positions. Oxide platelets can also be seen. Bar scale is 0.03 mm. (crossed nicols)

Plate 1.4. Photomicrograph of a clinopyroxene phenocryst showing orthopyroxene exsolution (this feature is termed as diallage). The lamellae are discontinuous, like an elongated eye with tapering ends and slight curvations along their length. Bar scale is 0.01 mm. (crossed nicols)

Plate 1.5. Photomicrograph of a clinopyroxene phenocryst showing thick orthopyroxene exsolution lamellae nearly parallel to the (100) plane. These lamellae are mostly discontinuous within the host, although continuous varieties are also seen. Bar scale is 0.03 mm. (crossed nicols)

Plate 1.6. Photomicrograph of a clinopyroxene phenocryst showing fine (continuous/discontinuous) orthopyroxene exsolution lamellae nearly parallel to the (100) plane. A portion of this phenocryst is enlarged in plate 1.7. Bar scale is 0.03 mm. (crossed nicols)

Plate 1.7. Photomicrograph of a clinopyroxene phenocryst showing the fine (continuous/discontinuous) (100) orthopyroxene exsolution lamellae. The fine (100) lamellae have a thicker and a thinner variety, with variable lamellae spacing. A closer look reveals that some of the thicker (100) lamellae show bulging along their length. Bar scale is 0.01 mm. (crossed nicols)

Plate 1.8. Photomicrograph of a clinopyroxene phenocryst showing both thick and thin orthopyroxene (100) exsolution lamellae, and thin pigeonite (001) exsolution lamellae. The closely spaced, discontinuous (001) lamellae cross cut both the continuous/discontinuous (100) lamellae. Oxide lamellae (bottom left of the photograph) can also be seen. Bar scale is 0.01 mm. (crossed nicols)

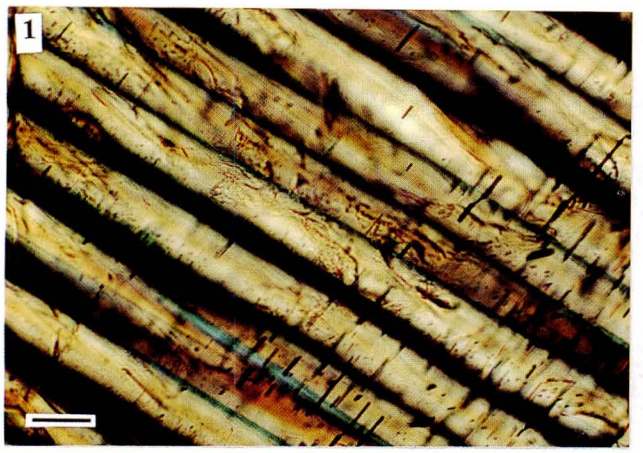
1

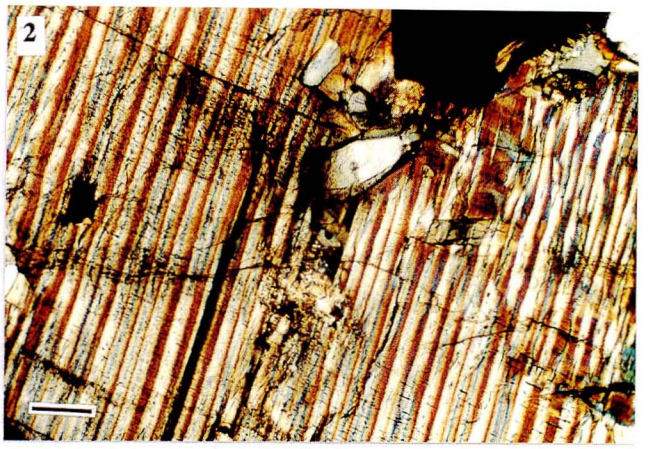
2


3

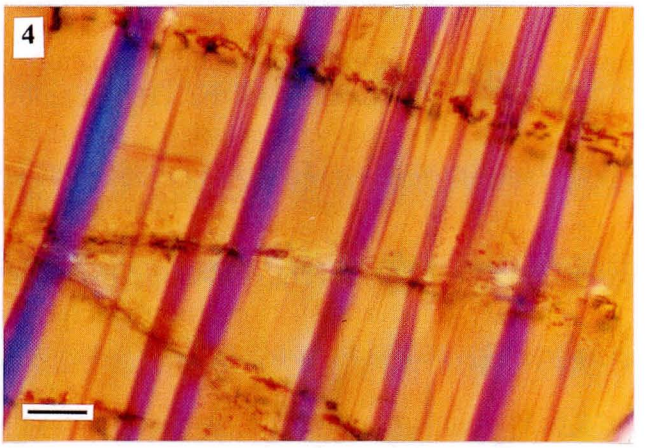
4

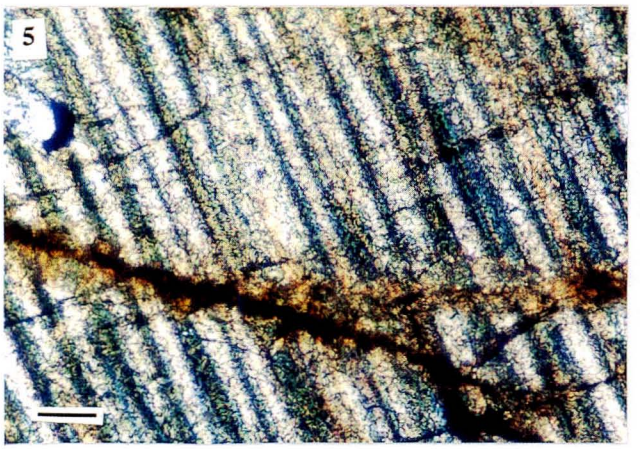
5

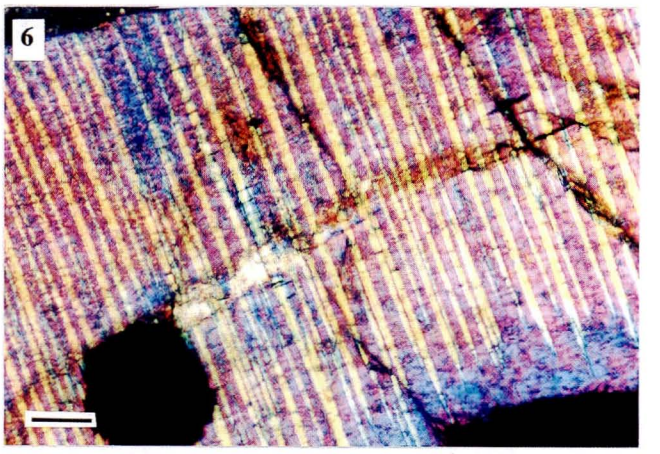
6

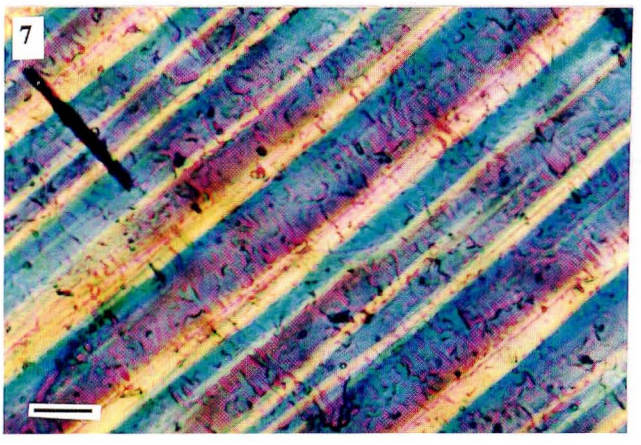
7

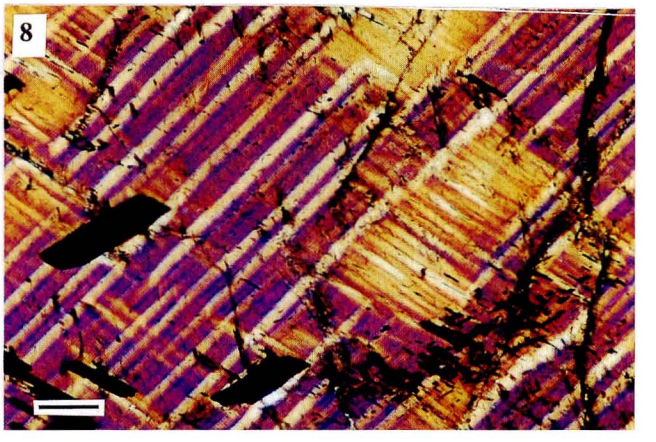
8

Plate 2

Plate 2.1. Photomicrograph of a clinopyroxene phenocryst showing two orientations of magnetite exsolution. They are distributed in the inner portions of the phenocryst. They usually occurs as rod-like and/or plate-like particles constituting isolated lamellae, though irregular particles are also common. Color imaging studies by EDX reveal that they are accompanied by much smaller dust-like particles of oxide lamellae. See text for details. Bar scale is 0.05 mm. (open nicols)

Plate 2.2. Photomicrograph of a clinopyroxene phenocryst showing magnetite and ilmenite platelets. The thick, rod-like to plate-like magnetite platelets have multiple orientations, while the needle-like ilmenite platelets occur in one direction. See text for details. Bar scale is 0.03 mm. (open nicols)

Plate 2.3. Photomicrograph of a clinopyroxene phenocryst showing two types of ilmenite lamellae, one nearly parallel to the (100) plane and the other slightly inclined to the (001) plane, and both are characterized by their slightly elongated plate-like shape. Both thick orthopyroxene (100) exsolution lamellae and thin pigeonite (001) exsolution lamellae can be seen. Bar scale is 0.03 mm. (crossed nicols)

Plate 2.4. Photomicrograph of a orthopyroxene phenocryst showing plagioclase exsolution parallel to (100) of the host. Note the relatively constant width and nearly uniform lamellar spacing. Minor oxide platelets can also be seen. Bar scale is 0.03 mm. (crossed nicols)

Plate 2.5. Photomicrograph of a orthopyroxene phenocryst showing plagioclase exsolution parallel to (100) of the host. The lamellae are sometimes discontinuous and show slight thickening and thinning along their lengths. Bar scale is 0.01 mm. (crossed nicols)

Plate 2.6. Photomicrograph of a orthopyroxene phenocryst showing plagioclase exsolution parallel to (100) of the host. Close observation of these plagioclase lamellae reveals that some of them are, in fact, discontinuous, containing segments of Fe-Ti oxide (ox) (ilmenite or magnetite) similar to the so-called combination lamellae. Fe-Ti oxide lamellae are also seen to post-date the plagioclase lamellae. Bar scale is 0.01 mm. (crossed nicols)

Plate 2.7. Photomicrograph of a orthopyroxene phenocryst showing blebby clinopyroxene exsolution. Bar scale is 0.03 mm. (crossed nicols)

Plate 2.8. Photomicrograph of a orthopyroxene phenocryst showing fine clinopyroxene exsolution lamellae, nearly parallel to (100). These lamellae constitute the most common lamellae of clinopyroxene in orthopyroxene phenocryst and are numerous, closely spaced and mostly continuous, although many are discontinuous. Bar scale is 0.03 mm. (crossed nicols)

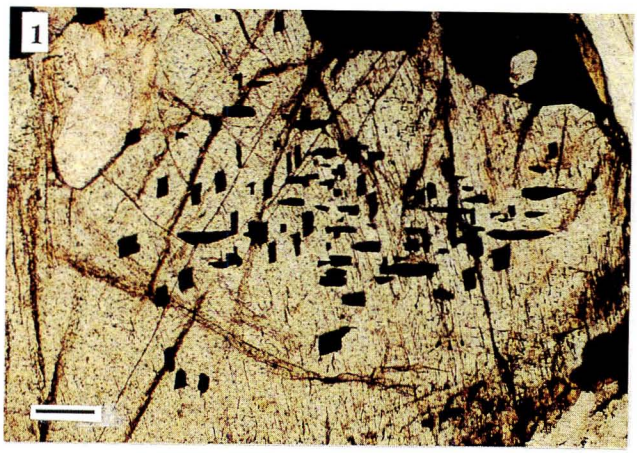
1


2

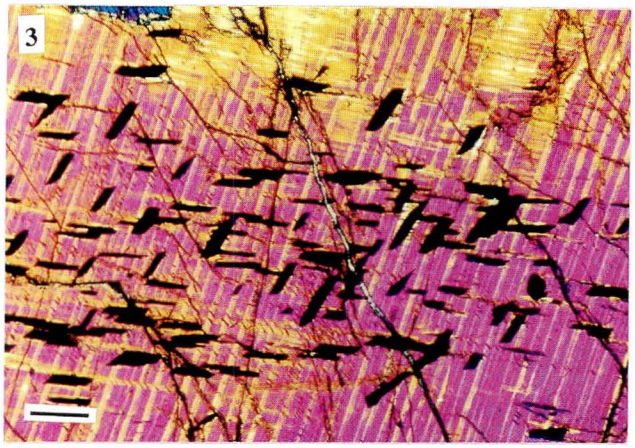
3

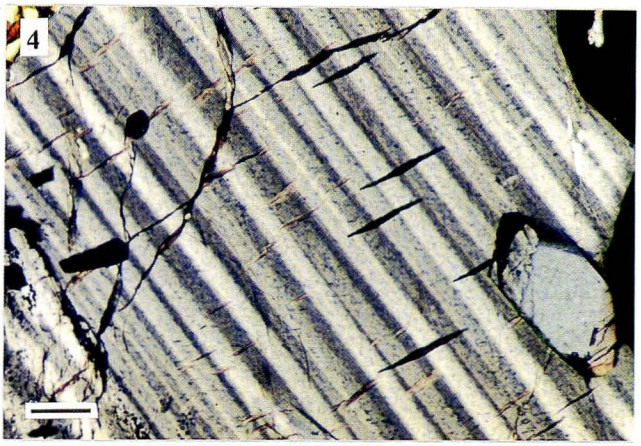
4

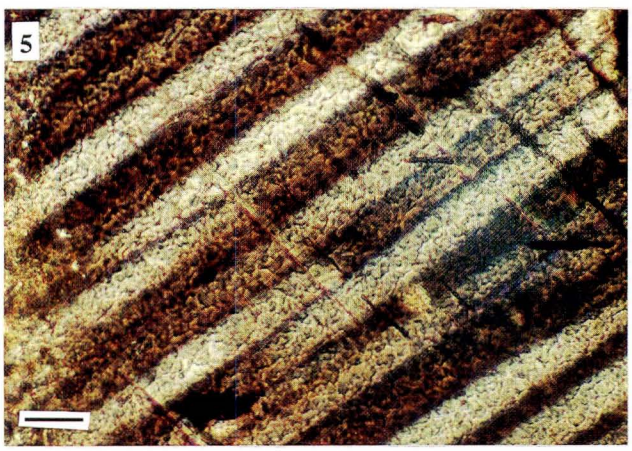
5

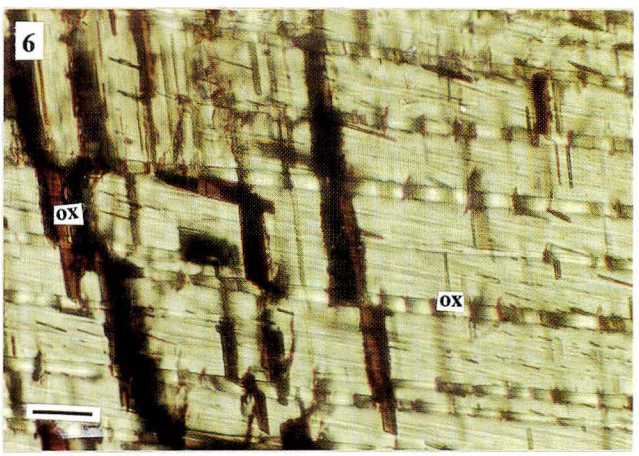
6
ox
ox

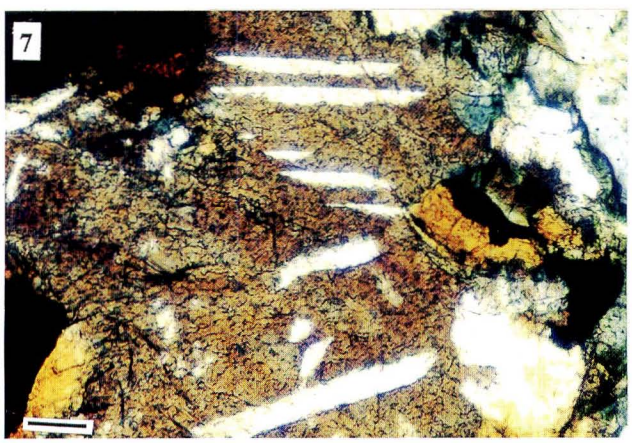
7

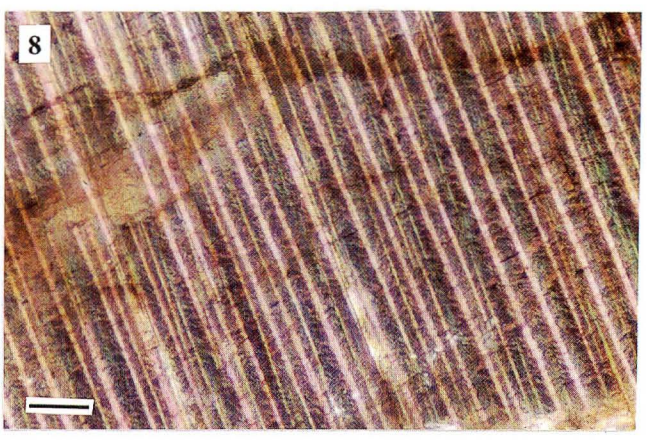
8

Plate 3

Plate 3.1. Photomicrograph of a orthopyroxene phenocryst showing fine, clinopyroxene exsolution lamellae nearly parallel to (100). These lamellae are sometimes thickened by the propagation of ledges along the (100) interface, as seen at the bottom left of the photograph (indicated by arrow). Bar scale is 0.01 mm. (crossed nicols)

Plate 3.2. Photomicrograph of a orthopyroxene phenocryst showing fine, clinopyroxene exsolution lamellae nearly parallel to (100). These lamellae are sometimes thickened by the propagation of ledges along the (100) interface. Bar scale is 0.01 mm. (crossed nicols)

Plate 3.3. Photomicrograph of a orthopyroxene phenocryst showing clinopyroxene exsolution nearly parallel to (001). These lamellae are characterized by their equal thickness and uniform distribution, and occur as both continuous and discontinuous varieties. Bar scale is 0.03 mm. (crossed nicols)

Plate 3.4. Photomicrograph of an inverted pigeonite in the host orthopyroxene phenocryst, with thick, widely spaced augite lamellae parallel to (001), and fine, relatively closely spaced augite lamellae parallel to (100). See text for details. Bar scale is 0.01 mm. (crossed nicols)

Plate 3.5. Photomicrograph of a orthopyroxene phenocryst showing two orientations of ilmenite exsolution. They are distributed in the inner portions of the phenocryst. They usually occurs as elongated rod-like and/or plate-like particles constituting isolated lamellae. Bar scale is 0.05 mm. (open nicols)

Plate 3.6. Photomicrograph of a orthopyroxene phenocryst showing one orientation of ilmenite exsolution. Clinopyroxene exsolution lamellae can also be seen. Note the small dust like oxide particles in between the larger ilmenite lamellae. Bar scale is 0.05 mm. (crossed nicols)

Plate 3.7. Photomicrograph of two adjacent orthopyroxene phenocrysts showing ilmenite (seen as elongated particles) and magnetite (seen as plate-like particles) exsolution. Bar scale is 0.1 mm. (crossed nicols)

Plate 3.8. Photomicrograph of a matrix clinopyroxene grain showing thin, exsolved platelets of oxide phases (either ilmenite or magnetite). Bar scale is 0.05 mm. (open nicols)

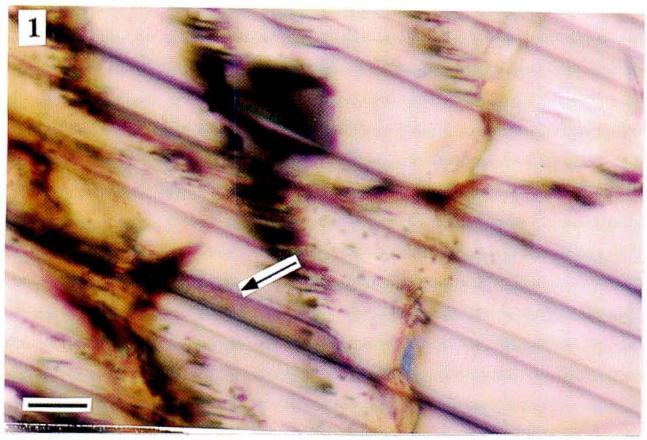
1

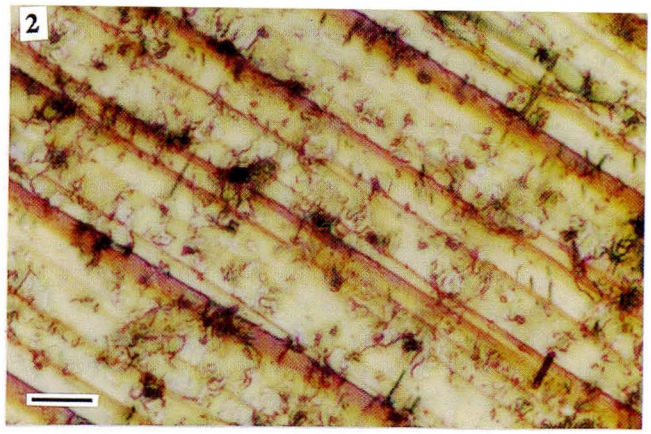
2

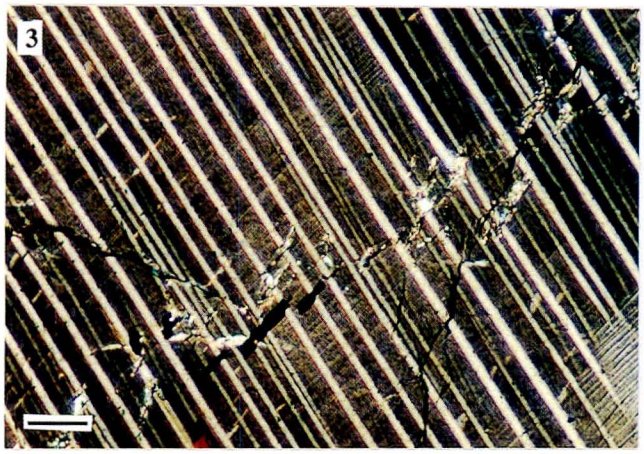
3

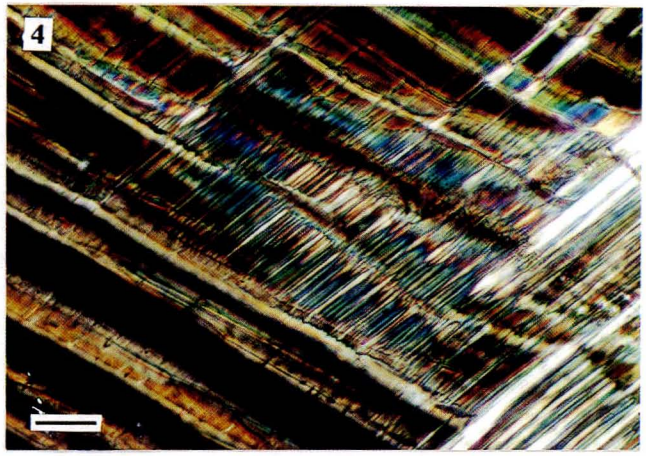
4

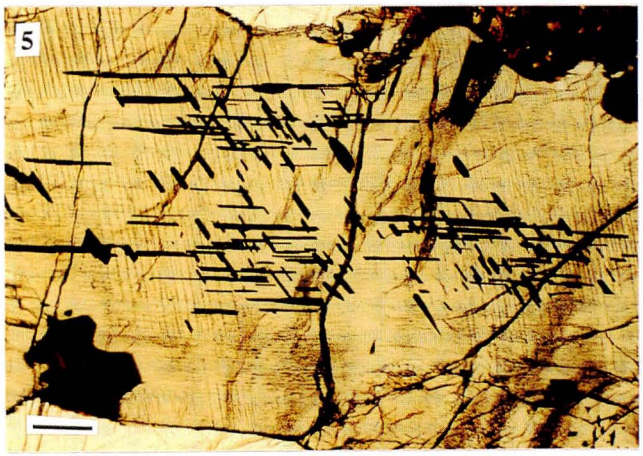
5

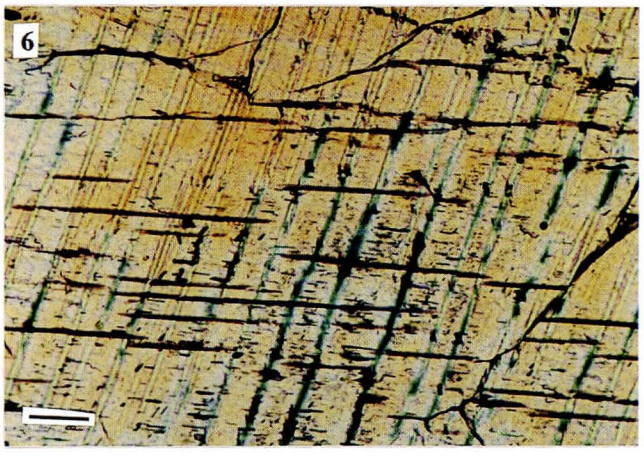
6

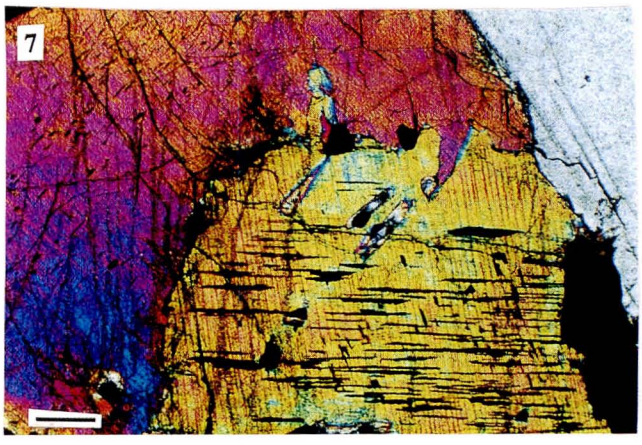
7

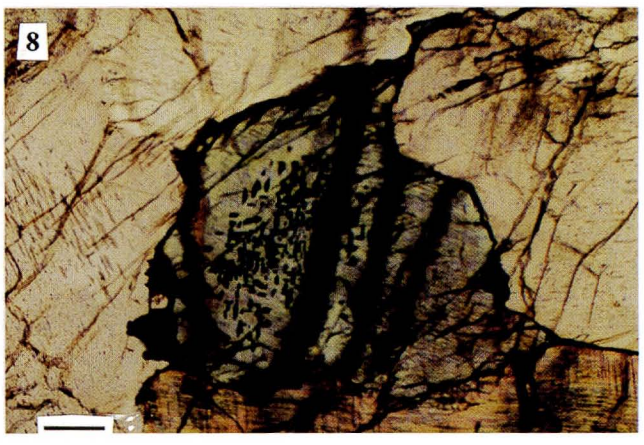
8